AD-A090 788 PANAMETRICS INC WALTHAM MASS F/G 4/1
BETASONDE II, A ROCKET-BORNE PROBE FOR ATMOSPHERIC DENSITY MEAS--ETC(U)
SEP 80 B SELLERS, J L HUNERWADEL DAAG29-76-C-0041
UNCLASSIFIED PANA-AIR-5 ARO-13870.1-GS NL

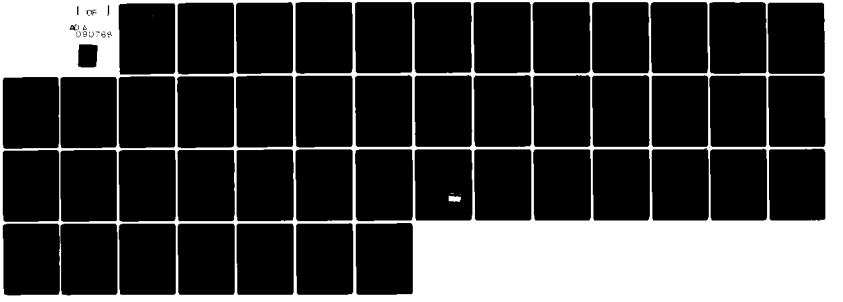

(12) ARO 13870.1-GS

LEVEL II

PANA-AIR-5

AD A090788

BETASONDE I, A ROCKET-BORNE PROBE FOR ATMOSPHERIC DENSITY MEASUREMENT IN THE MIDDLE ATMOSPHERE

Bach Sellers
Jean L. Hunerwadel

Panametrics, Inc.
221 Crescent Street
Waltham, Massachusetts 02154

September 1980

Final Report

GEOSCIENCES DIVISION
ARMY RESEARCH OFFICE
RESEARCH TRIANGLE PARK, NC 27709

80 10 22 037

Unclassified

SECURITY CLASSIFICATION OF THIS PAGE (When Data Entered)

REPORT DOCUMENTATION PAGE	READ INSTRUCTIONS BEFORE COMPLETING FORM
1. REPORT NUMBER: PANA-AIR-5	2. GOVT ACCESSION NO.: AD-A090788	3. RECIPIENT'S CATALOG NUMBER:
4. TITLE (and Subtitle): Betasonde II, A Rocket-Borne Probe for Atmospheric Density Measurement in the Middle Atmosphere	5. TYPE OF REPORT & PERIOD COVERED: Final, 1 May 1976-30 Sept 1979
	6. PERFORMING ORG. REPORT NUMBER:
7. AUTHOR(s): Bach/Sellers, Jean L./Hunerwadel	8. CONTRACT OR GRANT NUMBER(s): DAAG29-76-C-0041
9. PERFORMING ORGANIZATION NAME AND ADDRESS: Panametrics, Inc., 221 Crescent Street, Waltham, MA 02154	10. PROGRAM ELEMENT, PROJECT, TASK AREA & WORK UNIT NUMBERS:
11. CONTROLLING OFFICE NAME AND ADDRESS: Geosciences Division, Army Research Office, Research Triangle Park, NC 27709	12. REPORT DATE: September 1980
	13. NUMBER OF PAGES: 46
14. MONITORING AGENCY NAME & ADDRESS (if different from Controlling Office)	15. SECURITY CLASS. (of this report): Unclassified
	15a. DECLASSIFICATION DOWNGRADING SCHEDULE:

16. DISTRIBUTION STATEMENT (of this Report)

Approved for public release, distribution unlimited. Reproduction in whole or in part is permitted for any purpose of the United States Government.

17. DISTRIBUTION STATEMENT (of the abstract entered in Block 20, if different from Report)

18. SUPPLEMENTARY NOTES

The views, opinions, and/or findings contained in this report are those of the author(s) and should not be construed as an official Department of the Army position, policy, or decision unless so designated by other documentation.

19. KEY WORDS (Continue on reverse side if necessary and identify by block number)

Atmospheric density
Beta-ray scattering
Density gauge
Rocket sonde

20. ABSTRACT (Continue on reverse side if necessary and identify by block number)

A density gauge for use in the 20-90 km range of the atmosphere has been designed and fabricated. It is based on beta-ray forward scattering and uses a Pm-147 beta source. Estimated accuracy is ±6% or better for launch on an Arcas having apogee near 90 km. The flight model is now ready for integration into a rocket sonde. A flight program for the sonde is recommended, and techniques offering potential for application of the method up to 100 km are discussed.

DD FORM 1 JAN 73 1473 EDITION OF 1 NOV 65 IS OBSOLETE

Unclassified

i SECURITY CLASSIFICATION OF THIS PAGE (When Data Entered)

FOREWORD

The Betasonde was originally developed by Panametrics, Inc. under the sponsorship of the Division of Isotopes Development of the U.S.A.E.C. (Contract Monitor: Mr. John C. Dempsey) and the Atmospheric Sciences Branch of O.N.R. (Scientific Officer: Mr. James Hughes). Several launches of these early versions of the Betasonde were carried out at White Sands Missile Range, under the supervision of Mr. Harold N. Ballard of the Atmospheric Sciences Laboratory.

The advanced model Betasonde work reported here was supported by the Army Research Office and was monitored by Dr. Arthur V. Dodd of the Geosciences Division. The objective of the work was to develop a flight model of the Betasonde for integration into an Arcas rocket payload and application in a middle atmosphere flight program at White Sands Missile Range. This objective has been accomplished and the sonde is now available. However, the WSMR program in which the sonde was to be used was discontinued during the fabrication phase. Should funding be available for a flight program of density measurements up to 100 km, the Betasonde could be integrated into any of a variety of rockets and used for the purpose intended.

TABLE OF CONTENTS

LIST OF ILLUSTRATIONS

LIST OF TABLES

1. INTRODUCTION

1.1 Betasonde Development Summary

The importance of air density measurements has long been recognized. Furthermore, the importance is increasing due to the necessity of observing and forecasting atmospheric variables for re-entry, SST and other high performance vehicles. Under sponsorship of several Government Agencies, Panametrics, Inc. developed an Arcas borne sonde that utilizes beta ray forward scattering for density measurement up to about 60 km as shown below.

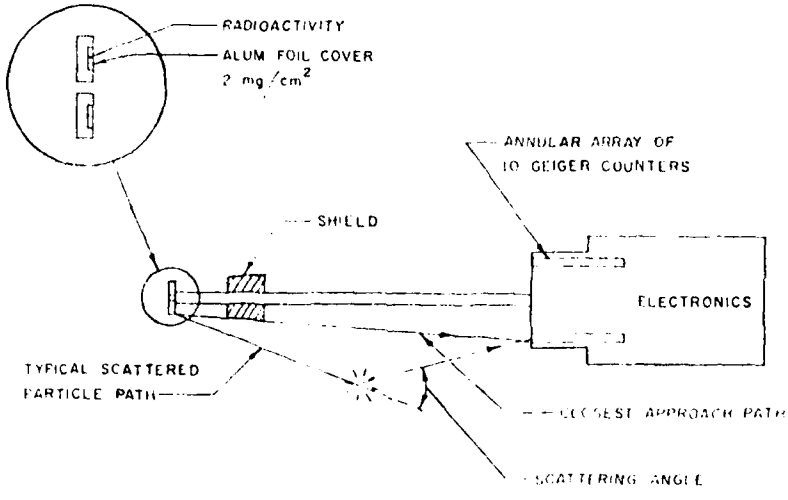

Figure 1.1 Cross Section of Original Betasonde Showing Density Measurement Concept

Essentially, a shield is interposed between an annular shaped beta source and a detector in such a manner that no direct-path beta particles can be detected. In the high altitude region ($\gtrsim$ 20 km), the detector counting rate is then almost linearly dependent on the atmospheric density, since only air-scattered particles can reach the detector.

Under AEC, ONR, WSMR and ARO sponsorship, there have been three models of this device designed and fabricated:

1) Original Betasonde
2) Low Background Betasonde (LBB)
3) Betasonde II.

The work is detailed in References 1.1 - 1.3. The original Betasonde used standard size geiger counters (which had a substantial cosmic ray background effect), whereas the LBB used miniature ones (the same type used in discovering the Van Allen Belts) to reduce this effect. Betasonde II uses a semiconductor detector, which has a very low cosmic ray background effect. It is the subject of the effort described in the present report.

All three were designed for flight on an Arcas rocket, and when integrated into it, appear essentially as above. The density measurements are made as the sonde descends by parachute; hence, it is recoverable and reusable. As the work has progressed, we have pushed the upper altitude limit higher with each model; Betasonde II could require use of a boosted Arcas with an apogee in the 90 - 100 km region, provided a sufficiently intense beta source is used. Results obtained with the original version are discussed in Ref. 1.3.

Modification of the original betasonde to use the miniature geiger counters was funded by White Sands Missile Range (WSMR) and ONR. It was flown very successfully to an altitude of about 65 km at WSMR on April 23, 1976, and a report (PANA-AIR-1, Ref. 1.2) is available. Those atmospheric density measurements are included in Ref. 1.1 (Figures 3.1 and 3.2, pg. 23 - 24).

During the development work on the LBB we became convinced that the technique could be extended to the 90 - 100 km region by use of a semiconductor detector and a more intense beta source ($\approx$500 mCi). Following submission of a proposal to the ARO in November, 1975, we began work on a planned three-phase Betasonde II effort:

Phase I - Research and Development

Phase II - Design and Fabrication

Phase III - Flight and Data Analysis

The ARO funding was for the first two phases, with WSMR expected to fund the third phase. Near the end of the second phase, however, we were informed that such atmospheric research can no longer be funded by WSMR.

Our progress through the first phase is detailed in the annual report, Ref. 1.1. That work is briefly summarized in the present work, along with details of the design and fabrication work in Phase II. That effort has now been completed, and we could undertake Phase III work at any time.

That work could be described as follows: the instrument must be integrated into an Arcas payload for launch at White Sands Missile Range (an alternate vehicle or range could, of course, be used), calibrated at

both Panametrics and in a large (40' - 60') chamber in order to verify the high altitude ($\gtrsim$ 70 km) portion of the calibration curve. The proper intensity beta source must be procured for this work. The Betasonde II should then be flown to the 80 - 90 km region at least twice, and the analytical fitting procedure described in PANA-AIR-2 (Ref. 1.1) should be applied to the data. This will form the basis for routine direct measurement of atmospheric density up to at least the 80 - 90 km region. Reports would be prepared and the results published.

We would like to point out that, due to the development of lower noise semiconductor detectors, the possibility exists that this technique could, in fact, be extended to the region slightly above 100 km. But we believe that such a further development, if desirable, should take place only after testing Betasonde II and determining its upper altitude limits.

1.2 Detailed Description of Betasonde II Work

The Scope-of-Work for the subject contract is as follows:

The Contractor, as an independent Contractor and not as an agent of the Government, shall provide the necessary management, facilities, services and materials, as required, to accomplish the research project entitled "ATMOSPHERIC DENSITY MEASUREMENT IN THE MIDDLE ATMOSPHERE" in accordance with the Contractor's proposal dated November 1975 and revised during April 1976 which is incorporated as part of this contract by reference. The Contractor shall use the types of personnel listed in Exhibit A, attached, at approximately the level of effort stated. The research to be conducted will include but will not necessarily be limited to the design and fabrication of an instrument utilizing beta radiation to measure atmospheric density to an elevation of 100 kilometers. The first phase of the research involves investigation of satisfactory beta radiation sources and detection. Space simulation chambers will be used to measure and calculate the density response to beta radiation. Based on the results, a density sonde will be designed and fabricated in the second phase of the work.

Thus, the work under this contract was divided into two phases, as described above, and both have been successfully completed.

Section 2 contains a description of the method of density measurement by use of beta-ray forward scattering. A technique is presented for utilizing an entire array of density measurements to determine the optimum fit to an analytic altitude dependent profile. Measurements made with the Low Background Betasonde are used to demonstrate the technique.

The design and fabrication work on Betasonde II are detailed in Section 3. As discussed in Sections 2 and 3, calibration results for Betasonde II yield similar density sensitivity to that for the LBB, provided the same radiation source is used. For atmospheric application, the principal difference between the two sondes is that Betasonde II has very low cosmic ray background sensitivity, and so has a higher ultimate altitude limit. To apply Betasonde II up to the 80 km region, it will be necessary to obtain the proper beta source having strength of about 500 mCi. The basic specifications for Betasonde II are given at the close of Section 3.

Section 4 contains a short summary of results accomplished in this program and the conclusions regarding potential application of Betasonde II.

2. ATMOSPHERIC DENSITY MEASUREMENT METHOD AND RESULTS

In this section the basic concept of measuring atmospheric density by use of beta-ray forward scattering is summarized, and the accuracy that can be expected in any single measurement is presented based, essentially, on the statistics of the counting process. In any actual flight of the sonde, there would be a long series of such measurements. Thus, results are next presented for a method that uses all of the measurements to find the best fit, in a least squares sense, to the usual exponential dependence of density on altitude. All of the results in this section have been given previously in more detail (Ref. 1.1, Sections 3 and 4).

2.1 Description of Method

The measurement of atmospheric density by beta-ray forward scattering relies upon the fact that, at low densities, the number of particles scattered by a gas surrounding a beta source is proportional to the density. The source and detector must be arranged in a geometry such that the particles can only be detected if they scatter from the gas, as in the forward scattering configuration shown in Figures 1.1 and 2.1. The single-scattering count rate $C_s(E_t)$ cps of the detector for the source and detector energy threshold E_t (the energy above which all electrons are counted) is found by integrating over all scattering angles θ into solid angles $d\Omega$:

$$C_s(E_t) = \rho (nN_o/M) \iint_{\Omega} \int_{E_t}^{\infty} S_s(E_t) B_s(E) d\sigma(E,\theta) dE \qquad (2.1)$$

Here ρ = atmospheric density, g/cm^3
N_o = Avogadro's number, 6.023×10^{23} molecules/(g-mole)
M = molecular weight of atmosphere, g-mole
n = number of atmospheric atoms/molecule
$d\sigma = f(\theta)F(E)d\Omega$ cm^2/atom

$F(E) = (1-\beta^2)/\beta^4$

$f(\theta) = (Z^2 r_o^2/4)\ \mathrm{Sin}^{-4}\theta/2\ \ \mathrm{cm}^2/(\mathrm{sr\text{-}atom})$

$\beta = v/c$ = ratio of beta particle velocity to that of light

Z = atomic number of atmosphere

r_o = classical electron radius, 2.82×10^{-13} cm

$S_s(E_t)$ = total emission rate of source for particles of energy greater than E_t, β/sec

$B_s(E)$ = spectrum for beta source of type s, normalized to unity from E_t to ∞, β/keV

E kinetic energy, keV

The cross section $d\sigma(E,\theta)$ for scattering of an electron of energy E (in the energy range of interest here, $\gtrsim$50 keV) through an angle θ is given by Evans (Ref. 2.1). As shown above, it is separable into two functions, the first depending only on E, and the second only on θ. Thus, as shown, the count rate is proportional to ρ, and

$$C_s(E_t) = K_s(E_t)\rho \ \ \mathrm{cps} \qquad (2.2)$$

Clearly, K_s depends only on the source, detector and geometry characteristics as given by the right hand side of Eq. (2.1). It can be determined analytically for any particular beta source and geometry. This has been done (Ref. 1.1, Section 4) with the result that for those sources presently available, Pm-147 is the best choice. It has a suitably long half life, 2.5 years, and a maximum energy of 225 keV-which is sufficiently high that about half of the emitted beta particles have energy in excess of the 50 keV threshold E_t (See Ref. 2.2 for beta spectra). Thus, for the

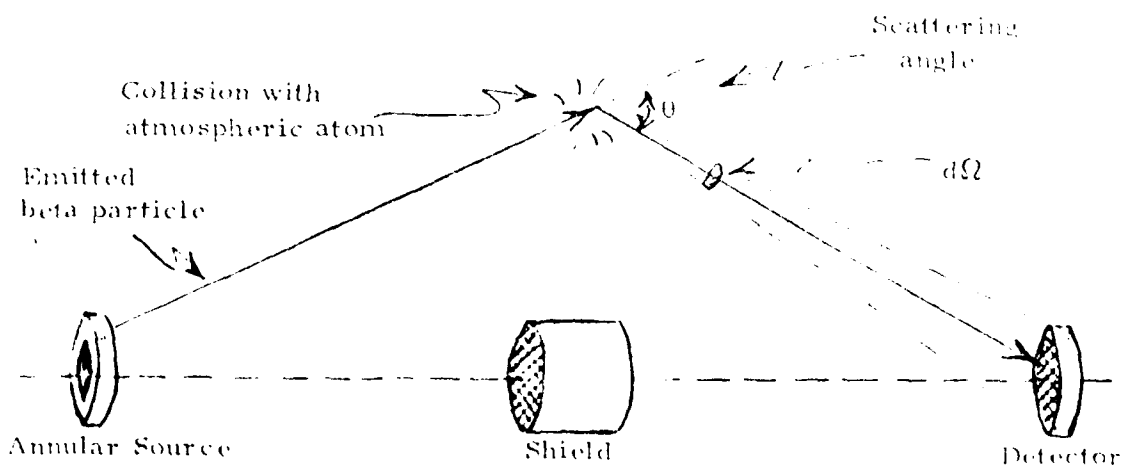

Figure 2.1 Beta-ray Scattering Configuration

present system, we believe that Pm-147 is optimum. It will provide a means of establishing the utility of the betasonde for the upper portion of the middle atmosphere. Results obtained by flight of a relatively low intensity Pm-147 source on the Low Background Betasonde (LBB) can be used to estimate the accuracy that would be obtained with higher intensity sources. Before doing this, it is necessary to discuss the experimental calibration procedure by which K_s can be determined for a particular sonde and source.

A difference between the present sonde and the LBB is that a significant wall effect is present during calibration in the Panametrics chamber (about 2'x3'). This was not experienced by the LBB due, we believe, to the extremely collimated geometry of the geiger counters themselves. Thus, going to the semiconductor detectors causes a significant increase in overall efficiency, but also produces a wall effect in the small chamber. This does not affect the determination of the constant K_s, since it is the slope of the count rate versus density curve. It does mean, however, that in order to obtain an actual calibration curve at densities less than that equivalent to about 70 km, it will be necessary to use a much larger chamber. Such chambers are available at NASA Langley Research Center (both 20' and 60' diameter spheres) and have been used previously (Ref. 1, 3) for betasonde calibration work.

Once it is established that a calibration measurement K_s in a small chamber leads to the same result as that obtained in a large chamber - in which the wall effect is much reduced - it is not then necessary to recalibrate in the large chamber unless the source-detector geometry is changed in some significant way. Rather, a value of K_s can be carefully measured in the small chamber in the $z \leq 60$ km region, where the wall effect is only a fraction of total count rate, even in the small chamber, and the calibration curve for higher altitudes can be obtained by extrapolation. This is possible because single-scattering is by far the dominant effect for $z \gtrsim 40$ km, hence the calibration curve is extremely linear and the count rate versus density is given rigorously by Eq. (2.2).

Thus, the calibration results in the small chamber can be used to estimate the accuracy obtainable at high altitudes and with a more intense source.

The source strength of the same annular Pm-147 beta source previously flown on the Low Background Betasonde (LBB) was measured on May 12, 1977 to be

$$S_s(E_t) \quad 2.76 \times 10^{9} \ \beta/\text{sec} \quad \underset{\text{(test source)}}{74.5 \text{ mCi}} \qquad (2.3)$$

for E_t = 50 keV. The slope of the count rate versus density, Eq. (2.2), was measured in the geometry of Fig. 1.1 to obtain the calibration constant

$$K_s(E_t) = 0.93 \times 10^9 \text{ cps}/(\text{g/cm}^3) \quad \text{(test source)} \tag{2.4}$$

for the source intensity (2.3). The efficiency of Betasonde II was found to be somewhat better than that of the LBB, but for purposes of illustration, we use the LBB calibration results.

Now, the fractional statistical uncertainty for any count rate C_s measured for a time t(sec) is given by (Ref. 1.2)

$$\Delta\rho/\rho = 1/\sqrt{C_s t} \tag{2.5}$$

By use of (2.2), this is

$$\Delta\rho/\rho = 1/\sqrt{K_s(E_t)\rho t} \tag{2.6}$$

This shows explicitly that the statistical uncertainty is a function of the threshold E_t through the calibration constant $K_s(E_t)$. Of course, K_s is also proportional to the source strength $S_s(E_t)$ through (2.1). We believe that a source of intensity about 5 times higher than (2.3) should be obtained to use as the first flight source,

$$S_s(E_t) = 1.38 \times 10^{10} \text{ } \beta/\text{sec} = 373 \text{ mCi}, \quad \text{(flight source)} \tag{2.7}$$

for which

$$K_s(E_t) = 4.65 \times 10^9 \text{ cps}/(\text{g/cm}^3). \quad \text{(flight source)} \tag{2.8}$$

Now, by use of the standard atmosphere densities (Ref. 2.3), Eqs. (2.2), (2.8) and (2.6), the following results are obtained:

Table 2.1

Estimated Fractional Statistical Uncertainty for Betasonde II and First Flight Source ($S_s \approx 373$ mCi)

Z km	ρ g/cm^3	C_s cps	$\Delta\rho/\rho$ t = 20 sec	t = 5 sec	t = 1 sec
60	3.1×10^{-7}	1441	.006	.012	.026
70	8.8×10^{-8}	409.2	.011	.022	.049
80	2.0×10^{-8}	93.0	.023	.046	.104
90	3.2×10^{-9}	14.9	.058	.116	.259
100	5.0×10^{-10}	2.3	.147	.295	.659

The uncertainties listed in this table are, of course, the minimum that will occur for the indicated count rates. The actual total error will be slightly larger due to some (as yet undetermined) cosmic ray effect. This is expected to be extremely small, however; much less than in the LBB (Ref. 1.2).

A typical rocket payload spends about 20 seconds within a 1 km region near apogee. As noted above, this allows a very accurate measurement of the density in that particular region. But as the payload descends, it initially gains speed until it is slowed by entry or, if the payload is to be recovered as for an Arcas, by a parachute. There is, then, a region in which the speed is high between apogee and entry. In this region the individual measurements, if assigned to altitude increments similar to those at higher and lower altitudes, are less accurate. Thus, a procedure has been developed that utilizes <u>all</u> of these measurements, with their associated accuracies, to define a density <u>profile</u>. This profile is, effectively, "tied" at high and low altitudes to some very accurate measurements, with the mid-altitude portion required to fit the less accurate data in that region and to fit smoothly with the profile for the other regions.

In the following sub-section, this procedure is summarized, and it is applied to results for a LBB flight to demonstrate its applicability.

2.2 Optimum Analytical Fit to Altitude-Density Profile

2.2.1 General Objective

As is well known, density $\rho(z)$ is approximately an exponentially decreasing function of altitude z:

$$\rho(z) = \rho_s e^{-z/H} \tag{2.9}$$

where H is the scale height and ρ_s the value of ρ at z 0. In fact, such an approximation is often made use of (Ref. 2.4, p 67) to provide analytical representations of models, for use in applications where such an approach is more convenient than is a long tabulation, for example where a computation is to be made that requires a continuous representation versus altitude. The result is generally provided in the form of the coefficients in a power series expansion for $\ln\rho(z)$. We believe that a similar approach could also be useful for representing the data from a single determination of a $\rho(z)$ profile, in particular, from a rocket launch such as that of Betasonde II, the instrument developed under the present contract for air density measurement up to at least 80 km by beta ray forward scattering.

The Low-Background Betasonde (LBB) is an earlier version Areas borne instrument designed, principally, for measurement of $\rho(z)$ between about 25 and 65 km. The direct output of the data reduction procedure is a tabulation of individual densities $\rho_i(z)$ and associated statistical uncertainties, $\Delta\rho_i(z)$, versus z_i. When making use of data of this type it is normally not possible simply to interpolate directly between values in the tabulation. The reason is that the points, when plotted, will generally show an amount of scatter consistent with the uncertainties. Thus, in order to use such data it is necessary to draw a best-fit curve of some type on the plot (usually simply by eye). Values are then read off the curve and assumed to have an uncertainty consistent with that of the statistical $\Delta\rho_i(z)$, and any additional systematic errors, in that altitude region. Clearly, then, determination of an optimum analytical fit for a tabulation would serve two purposes. It would provide a "formal" method of fitting the data, and the resulting analytical fit would provide a convenient representation for computational purposes.

We will use the results of a launch of the LBB at White Sands Missile Range at 17:09:00 UT on April 23, 1976 (Ref. 1.2) to show the type analytical fit that can be obtained. First the general mathematical approach is presented, and this is followed by the density tabulation and the application of the approach to the tabulation to determine the optimum fit.

2.2.2 Mathematical Approach

The deviation of (2.9) from an exact exponential can be taken into account by allowing the scale height H to be a function of altitude. Over the altitude region up to about 100 km, H is not strongly dependent on z and should be representable as a simple function (this is essentially what is done in the standard approach to model fitting). By doing this the result H(z) is a physically meaningful parameter, although for a given analytical fit the dependence on z can be expected to agree with model results in only an approximate manner. For purposes of determining a fit over a particular altitude region it is then convenient, and appropriate, to use

$$\rho = \rho_o e^{-(z - z_o)/\bar{H}(z)} \tag{2.10}$$

where z_o is the (specified) minimum altitude of interest. ρ_o is the value of ρ at $z = z_o$ and $\bar{H}(z)$ is an "average" value of H(z), as determined by the fitting procedure. Thus, once ρ_o and $\bar{H}(z)$ are found from the procedure, the analytical result (2.10) represents the entire array of measured density profile data, which are in the form ρ_i and statistical uncertainty $\Delta\rho_i$ for all N altitudes z_i. The procedure is used to minimize the sum of the mean squared fractional deviations D_i of all ρ values, calculated from (2.10) from the measured results ρ_i:

$$D_i = (\rho - \rho_i)/\rho = 1 - \rho_i/\rho \tag{2.11}$$

In order to determine how well the fit has been made, once the procedure is complete, it is useful to compare two quantities. The first is the rms uncertainty Δ_m of the N values of fractional uncertainty Δ_i in the individual measurement,

$$\Delta_m^2 = \sum_{i=1}^{N} \Delta_i^2/N \tag{2.12}$$

where

$$\Delta_i = \Delta\rho_i/\rho_i \tag{2.13}$$

and $\Delta\rho_i$ is the statistical uncertainty (Ref. 1.2, p 18). The second quantity is

$$\Delta_c^2 = \sum_i (\rho_i/\rho(z_i) - 1)^2/N \tag{2.14}$$

which is the rms deviation of the $\rho(z_j)$ values, calculated by use of (2.10), from the measured values ρ_j. If all measurements were made at only one value of ρ, then it would be expected that $\Delta_m \approx \Delta_c$. This is because, for a given actual ρ, the random variations in the measured ρ_j for the Betasonde are due to the statistical nature of the nuclear decay process that leads to beta emission. The values of ρ_j are distributed in a Poisson-like manner, for which the fractional standard deviation of the mean of a series of N readings would be given by (2.12). The Pearson "chi-squared" test can readily be applied in such circumstances to determine how well the measurements fit the distribution assumed. Here, however, we are dealing with the comparison of a best analytical fit (rather than the mean of a series of measurements) to the individual measurements, each of which is expected to be slightly different because z is changing. Additionally, some atmospheric variability will exist that cannot be fitted by a simple function such as (2.10) without an unrealistically large amount of variation in $\bar{H}(z)$, and this will in itself cause Δ_c to exceed Δ_m. Clearly, in this case we expect $\Delta_c > \Delta_m$, and we can conclude that the fit is satisfactory if the difference is acceptably small.

Thus, the procedure here is to find the simplest possible representation of $\bar{H}(z)$ that will produce a value of Δ_c that is acceptably close to Δ_m. A fit in which $\Delta_c \ll \Delta_m$ would not represent a true best fit; this could be obtained by using a sufficiently complicated function for $H(z)$ and would correspond to following the random deviations in the measurements, rather than the true average variation of $\rho(z)$. The question of exactly how closely Δ_c must approach Δ_m for the analytical fit to represent the experimental tabulation acceptably is not considered further here. Rather, we showed (Ref. 1.2) that fits can be obtained in which the difference is small and reduces in the manner expected as the number of A_j increases.

For the fit used here, a set of coefficients A_j was determined in which we represent $\bar{H}(z)$ in an inverse power series, so that

$$\ln(1/\rho_o) \qquad A_1 \tag{2.15}$$

$$(z - z_o)/\bar{H}(z) \qquad \sum_{j=2}^{j_m} A_j (z - z_o)^{j-1} \tag{2.16}$$

and j_m is the number of coefficients A_j chosen to be used. Clearly, once all A_j are known, both ρ_o and $\bar{H}(z)$ can be found from (2.15) and (2.16):

$$\rho_o = e^{-A_1} \tag{2.17}$$

$$\bar{H}(z) = 1 \Big/ \sum_{j=2}^{j_m} A_j (z - z_o)^{j-2} \tag{2.18}$$

Hence, a fit must be made to determine the A_j for use in (2.17) and (2.18), which then defines $\rho(z)$ from (2.10).

2.2.3 Flight Data and Density Tabulation

Details of the Low Background Betasonde (LBB) flight on April 23, 1970, are contained in Ref. 1.2 and presented here only to the extent necessary for application of the above procedure.

The Arcas was launched to an apogee altitude near 65 km, with the parachute borne LBB being ejected just before apogee. The parachute has little effect above 50 km. The descent velocity changes from about .2 km/sec to .02 km/sec between 60 and 30 km. However, the sonde does spend nearly 20 seconds within 1 km of apogee, thus providing much data in this region before beginning its rapid descent. This is an important fact, because it allows the density profile to be "tied down" at high altitude. Clearly, as the sonde descent rate slows, it obtains progressively more data in each altitude region. Hence, the entire density profile for the low altitude region is very accurately defined. The procedure described above is designed such that it provides a single analytical fit that automatically takes all of these factors into account.

The Betasonde pulses, each of which (except for cosmic ray background) corresponds to detection of an air-scattered beta particle, are telemetered and recorded on magnetic tape in real-time. These pulses are then summed into approximately equal time intervals t_m - dependent upon telemetry noise and time used for transmitting temperature for diagnostic purposes. In Table 2.2 these sums are labelled CTS at each altitude z(km) for the time interval TM(SEC'S). These are the basic data from which the density measurement at each altitude is determined.

Table 2.2 Low Background Betasonde Count Data for April 23, 1976 Flight

Z(KM)	TM(SECS)	CTS
64.0	5.5	80.
64.3	5.2	89.
64.2	5.4	85.
63.5	5.2	83.
62.9	5.1	102.
62.1	5.1	99.
61.0	5.2	130.
60.0	5.2	133.
59.1	5.1	156.
57.9	5.1	155.
55.9	5.1	219.
54.9	5.1	240.
53.9	5.1	259.
53.0	5.1	279.
52.0	5.0	355.
51.2	5.2	376.
50.5	5.0	376.
50.0	4.1	311.
49.5	4.0	361.
48.6	5.0	543.
48.1	5.0	502.
47.7	5.1	565.
47.2	4.0	467.
46.8	4.0	485.
46.4	4.1	495.
45.8	2.0	307.
45.3	4.0	650.
45.0	4.0	626.
44.2	4.0	683.
43.9	4.0	748.
43.4	5.0	1047.
43.1	5.1	989.
42.8	5.0	1093.
42.5	5.0	1124.
42.2	5.1	1197.
41.9	4.0	942.
41.7	4.0	1024.
41.1	5.0	1408.
40.8	5.0	1443.
40.5	5.0	1510.
40.2	5.1	1538.
40.0	5.0	1610.
39.7	5.0	1652.
39.5	5.0	1742.
39.3	5.0	1803.
39.0	4.0	1507.
38.5	4.1	1574.
38.3	5.0	2007.
38.1	5.0	2086.
37.9	5.0	2228.
37.6	5.0	2241.
37.4	5.0	2335.
37.2	5.0	2385.
37.0	5.0	2400.
36.8	5.0	2545.
36.2	5.0	2808.
36.1	5.0	2964.
35.9	5.0	2975.
35.7	5.0	2890.
35.5	5.0	3102.
35.4	5.0	3098.
35.2	5.0	3166.
35.1	5.0	3344.
34.9	4.0	2655.
34.5	5.1	3547.
34.4	5.0	3628.
34.3	5.0	3530.
34.1	5.0	3444.
34.0	5.0	3666.
33.9	5.0	3809.
33.7	5.0	3829.
33.6	5.0	4038.
33.5	4.0	3283.
33.1	5.0	4097.
33.0	5.1	4227.
32.9	5.0	4359.
32.8	5.0	4363.
32.6	5.0	4580.
32.4	5.0	4735.
32.2	5.0	4755.
32.1	5.0	4895.
32.0	4.0	3944.
31.6	5.0	5055.
31.5	5.0	5353.
31.3	5.1	5316.
31.2	5.0	5271.
31.0	5.0	5406.
30.8	5.0	5701.
30.7	5.0	5707.
30.5	5.0	5901.
30.4	4.0	4735.
30.0	5.0	6338.
29.9	5.0	6418.
29.7	5.0	6332.
29.6	5.0	6350.
29.5	5.0	6462.
29.3	5.0	6764.
29.1	5.0	6708.
29.0	5.0	6757.
28.9	4.0	5757.
28.6	5.0	6895.
28.5	5.1	7383.
28.3	5.0	7335.
28.2	5.0	7454.
28.1	5.0	7724.
27.9	5.0	7764.
27.7	5.0	7901.
27.6	5.0	7773.
27.4	4.0	6502.
27.2	5.0	8424.
27.1	4.0	6541.
27.0	5.0	8401.
26.9	5.0	8239.
26.7	5.0	8719.
26.6	5.0	8675.
26.5	5.1	8509.
26.3	5.0	8914.
26.2	5.0	8892.

It is seen that the counts generally increase as altitude decreases, because the number of beta particles scattered increases as the density increases in this density region. In addition to the density itself, there are several other factors that must be taken into account in determining density from this count rate (see Ref. 1.2 for details of procedure):

1) circuit dead-time, caused by dead time in geiger counters after counting a pulse ($\approx 25\mu$sec) and a dead-time circuit introduced purposely to keep the count rate into the telemetry transmitter from exceeding its capabilities,

2) cosmic ray effect, a small, but non-negligible, altitude-dependent effect,

and 3) time elapsed between calibration and flight.

Each of these factors has been taken into account as necessary in obtaining the calibration data of Table 2.3 and the flight density tabulation in Table 2.4. In the latter table the count data from Table 2.2 are repeated as the first three columns, with the observed counts (OBSCTS) in the third. This leads to an observed count rate (not shown) which is corrected for dead time, by use of the circuit dead time of 185μsec, to obtain the corrected count rate (CORCTR). The cosmic ray count rate (COSCTR) is then subtracted to obtain the density-dependent count rate (DENCTR).

The last of the factors that must be taken into account is important because of decay in intensity of the radioactive source, in this case Pm-147 whose mean life is 1378 days. Essentially, a calibration curve that would be correct on the day of the flight is derived from that recorded earlier. In the present instance, the time lapse was only 16 days, and the calibration data are shown in Table 2.3. There are 22 points at which the density ρ(g/m^3) and the count rate, corrected for the dead time factor, was as shown in CTS/SEC. At low values of ρ, the count rate increases approximately linearly, but as ρ increases the count rate increases less rapidly. At 25 km $\rho \approx 40$ g/m^3 and at 30 km $\rho \approx 20$ g/m^3. Data below about 30 km were not analyzed in Ref. 1.2 because of the non-linear nature of the calibration curve in that region. Here, however, all of the data in Table 2.2 are analyzed. This was done by making, for each flight count rate, a quadratic fit to three appropriate calibration count rate points in Table 2.3. The measured DENSITY values of Table 2.4 were thus determined from the density-dependent count rate DENCTR, and the analytical fit to the density - count rate results in Table 2.3.

The absolute uncertainty, UNC (g/m^3) is obtained from the density, the counts, and the calibration data. The fractional uncertainty Δ_i is given by the ratio UNC/DENSITY.

Table 2.3 Low Background Betasonde Density Calibration Data Recorded April 7, 1976.

PT	RHO(G/M**3)	CTS/SEC
01	00	0000.
02	02	0174.
03	04	0352.
04	06	0524.
05	08	0700.
06	10	0874.
07	12	1045.
08	14	1220.
09	16	1400.
10	18	1575.
11	20	1750.
12	22	1900.
13	24	2020.
14	26	2130.
15	28	2245.
16	30	2345.
17	32	2440.
18	34	2530.
19	36	2620.
20	38	2705.
21	40	2790.
22	42	2880.

Table 2.4 Low Background Betasonde Measured Density Tabulation for April 23, 1976 Flight

MEAN-LIFE,DAYS=1378.
TIME FROM CAL,DAYS=16.
CIR. DEAD TIME,SEC=.000185

UNITS:ALT=KM;TIME-INT=SEC;ALL CTR=CPS;DEN,UNC=G/M**3

ALT	TIME-INT	OBSCTS	CORCTR	COSCTR	DENCTR	DENSITY	UNC	FRAC-UNC
64.0	5.5	80.	14.58	0.30	14.45	0.168	0.019	0.112
64.3	5.2	89.	17.17	0.30	17.07	0.198	0.021	0.106
64.2	5.4	85.	15.79	0.30	15.67	0.182	0.020	0.108
63.5	5.2	83.	16.01	0.30	15.89	0.185	0.020	0.110
62.9	5.1	102.	20.07	0.30	20.01	0.232	0.023	0.099
62.1	5.1	99.	19.48	0.30	19.41	0.225	0.023	0.100
61.0	5.2	130.	25.12	0.30	25.11	0.291	0.026	0.088
60.0	5.2	133.	25.70	0.30	25.70	0.298	0.026	0.087
59.1	5.1	156.	30.76	0.30	30.82	0.357	0.029	0.080
57.9	5.1	155.	30.56	0.30	30.62	0.355	0.028	0.080
55.9	5.1	219.	43.29	0.30	43.49	0.504	0.034	0.067
54.9	5.1	240.	47.47	0.30	47.72	0.553	0.036	0.064
53.9	5.1	259.	51.27	0.30	51.56	0.597	0.037	0.062
53.0	5.1	279.	55.27	0.30	55.61	0.644	0.038	0.060
52.0	5.0	355.	71.94	0.30	72.48	0.839	0.044	0.053
51.2	5.2	376.	73.29	0.30	73.84	0.854	0.044	0.051
50.5	5.0	376.	76.26	0.30	76.85	0.889	0.046	0.051

Table 2.4 (Cont.)

ALT	TIME-INT	OBSCTS	CORCTR	COSCTR	DENCTR	DENSITY	UNC	FRAC-UNC
50.0	4.1	311.	76.93	0.30	77.53	0.897	0.051	0.056
49.5	4.0	361.	91.78	0.31	92.54	1.069	0.056	0.052
48.6	5.0	543.	110.83	0.32	111.80	1.290	0.055	0.043
48.1	5.0	502.	102.30	0.32	103.17	1.191	0.053	0.044
47.7	5.1	565.	113.10	0.33	114.09	1.316	0.055	0.042
47.2	4.0	467.	119.33	0.33	120.38	1.388	0.064	0.046
46.8	4.0	485.	124.03	0.34	125.14	1.443	0.065	0.045
46.4	4.1	495.	123.49	0.34	124.58	1.437	0.064	0.045
45.8	2.0	307.	157.99	0.35	159.48	1.835	0.104	0.056
45.3	4.0	650.	167.54	0.36	169.13	1.945	0.075	0.039
45.0	4.0	626.	161.17	0.36	162.68	1.871	0.074	0.040
44.2	4.0	683.	176.32	0.37	178.00	2.044	0.075	0.037
43.9	4.0	748.	193.70	0.37	195.58	2.239	0.079	0.035
43.4	5.0	1047.	217.84	0.38	220.00	2.510	0.076	0.030
43.1	5.1	989.	201.14	0.38	203.10	2.322	0.072	0.031
42.8	5.0	1093.	227.81	0.39	230.08	2.622	0.078	0.030
42.5	5.0	1124.	234.55	0.39	236.90	2.699	0.079	0.029
42.2	5.1	1197.	245.36	0.40	247.82	2.821	0.080	0.028
41.9	4.0	942.	246.23	0.40	248.70	2.831	0.091	0.032
41.7	4.0	1024.	268.73	0.40	271.46	3.086	0.095	0.031
41.1	5.0	1408.	297.08	0.41	300.13	3.410	0.091	0.027
40.8	5.0	1443.	304.88	0.41	308.02	3.499	0.092	0.026
40.5	5.0	1510.	319.87	0.42	323.19	3.671	0.095	0.026
40.2	5.1	1538.	319.39	0.42	322.69	3.666	0.094	0.026
40.0	5.0	1610.	342.40	0.42	345.97	3.931	0.098	0.025
39.7	5.0	1652.	351.91	0.43	355.59	4.042	0.103	0.025
39.5	5.0	1742.	372.40	0.43	376.32	4.285	0.106	0.025
39.3	5.0	1803.	386.38	0.43	390.45	4.451	0.108	0.024
39.0	4.0	1507.	404.98	0.43	409.27	4.671	0.123	0.026
38.5	4.1	1574.	413.25	0.44	417.63	4.768	0.123	0.026
38.3	5.0	2007.	433.60	0.44	438.21	5.008	0.114	0.023
38.1	5.0	2086.	452.09	0.45	456.92	5.225	0.116	0.022
37.9	5.0	2228.	485.63	0.45	490.85	5.618	0.120	0.021
37.6	5.0	2241.	488.72	0.45	493.97	5.654	0.120	0.021
37.4	5.0	2335.	511.16	0.45	516.67	5.916	0.123	0.021
37.2	5.0	2385.	523.17	0.46	528.81	6.054	0.122	0.020
37.0	5.0	2400.	526.78	0.46	532.47	6.096	0.123	0.020
36.8	5.0	2545.	561.91	0.46	568.01	6.498	0.128	0.020
36.2	5.0	2808.	626.71	0.47	633.56	7.242	0.136	0.019
36.1	5.0	2964.	665.82	0.47	673.12	7.693	0.141	0.018
35.9	5.0	2975.	668.60	0.47	675.93	7.725	0.141	0.018
35.7	5.0	2890.	647.21	0.48	654.28	7.478	0.139	0.019
35.5	5.0	3102.	700.84	0.48	708.54	8.097	0.145	0.018
35.4	5.0	3098.	699.82	0.48	707.51	8.086	0.145	0.018
35.2	5.0	3166.	717.22	0.48	725.11	8.286	0.147	0.018
35.1	5.0	3344.	763.23	0.48	771.66	8.819	0.153	0.017
34.9	4.0	2655.	756.66	0.49	765.01	8.743	0.170	0.019
34.5	5.1	3547.	798.19	0.49	807.02	9.226	0.156	0.017
34.4	5.0	3628.	838.10	0.49	847.39	9.692	0.163	0.017
34.3	5.0	3530.	812.06	0.49	821.05	9.388	0.159	0.017
34.1	5.0	3444.	789.39	0.50	798.11	9.123	0.156	0.017

Table 2.4 (Cont.)

ALT	TIME-INT	OBSCTS	CORCTR	COSCTR	DENCTR	DENSITY	UNC	FRAC-UNC
34.0	5.0	3666.	848.26	0.50	857.66	9.811	0.164	0.017
33.9	5.0	3809.	886.78	0.50	896.63	10.267	0.171	0.017
33.7	5.0	3829.	892.20	0.50	902.11	10.332	0.172	0.017
33.6	5.0	4038.	949.45	0.50	960.04	11.012	0.177	0.016
33.5	4.0	3283.	967.68	0.50	978.47	11.227	0.199	0.018
33.1	5.0	4097.	965.81	0.51	976.57	11.205	0.178	0.016
33.0	5.1	4227.	978.92	0.51	989.84	11.360	0.177	0.016
32.9	5.0	4359.	1039.44	0.51	1051.07	12.070	0.184	0.015
32.8	5.0	4363.	1040.58	0.51	1052.22	12.084	0.184	0.015
32.6	5.0	4580.	1102.90	0.51	1115.26	12.810	0.189	0.015
32.4	5.0	4735.	1148.15	0.52	1161.04	13.332	0.192	0.014
32.2	5.0	4755.	1154.04	0.52	1166.99	13.400	0.192	0.014
32.1	5.0	4895.	1195.53	0.52	1208.96	13.876	0.195	0.014
32.0	4.0	3944.	1205.98	0.52	1219.54	13.995	0.219	0.016
31.6	5.0	5055.	1243.60	0.53	1257.59	14.413	0.195	0.014
31.5	5.0	5353.	1335.01	0.53	1350.07	15.439	0.206	0.013
31.3	5.1	5316.	1291.38	0.53	1305.92	14.947	0.199	0.013
31.2	5.0	5271.	1309.61	0.53	1324.37	15.153	0.203	0.013
31.0	5.0	5406.	1351.54	0.53	1366.78	15.627	0.208	0.013
30.8	5.0	5701.	1445.00	0.54	1461.34	16.701	0.221	0.013
30.7	5.0	5707.	1446.93	0.54	1463.29	16.723	0.221	0.013
30.5	5.0	5901.	1509.86	0.54	1526.95	17.451	0.227	0.013
30.4	4.0	4735.	1515.67	0.54	1532.83	17.518	0.255	0.015
30.0	5.0	6338.	1655.92	0.55	1674.71	19.096	0.243	0.013
29.9	5.0	6418.	1683.33	0.55	1702.44	19.421	0.253	0.013
29.7	5.0	6332.	1653.88	0.55	1672.64	19.072	0.243	0.013
29.6	5.0	6350.	1660.02	0.55	1678.85	19.144	0.245	0.013
29.5	5.0	6462.	1698.50	0.55	1717.78	19.605	0.258	0.013
29.3	5.0	6764.	1804.38	0.55	1824.89	20.929	0.296	0.014
29.1	5.0	6708.	1784.51	0.56	1804.79	20.666	0.283	0.014
29.0	5.0	6757.	1801.89	0.56	1822.37	20.896	0.294	0.014
28.9	4.0	5757.	1961.53	0.56	1983.87	23.378	0.444	0.019
28.6	5.0	6895.	1851.29	0.56	1872.34	21.589	0.327	0.015
28.5	5.1	7383.	1977.16	0.56	1999.68	23.648	0.400	0.017
28.3	5.0	7335.	2013.44	0.57	2036.38	24.303	0.439	0.018
28.2	5.0	7454.	2058.54	0.57	2082.01	25.138	0.437	0.017
28.1	5.0	7724.	2162.94	0.57	2187.63	26.962	0.433	0.016
27.9	5.0	7764.	2178.66	0.57	2203.53	27.242	0.445	0.016
27.7	5.0	7901.	2232.98	0.57	2258.48	28.263	0.498	0.018
27.6	5.0	7778.	2184.17	0.57	2209.10	27.341	0.449	0.016
27.4	4.0	6502.	2324.53	0.58	2351.09	30.125	0.599	0.020
27.2	5.0	8424.	2447.73	0.58	2475.73	32.794	0.599	0.018
27.1	4.0	6541.	2344.52	0.58	2371.31	30.542	0.609	0.020
27.0	5.0	8401.	2438.03	0.58	2465.91	32.576	0.598	0.018
26.9	5.0	8239.	2370.40	0.58	2397.49	31.091	0.558	0.018
26.7	5.0	8719.	2574.27	0.59	2603.74	35.629	0.632	0.018
26.6	5.0	8675.	2555.13	0.59	2584.38	35.194	0.620	0.018
26.5	5.1	8509.	2413.33	0.59	2440.92	32.020	0.588	0.018
26.3	5.0	8914.	2660.17	0.59	2690.64	37.662	0.671	0.018
26.2	5.0	8892.	2650.39	0.59	2680.74	37.429	0.669	0.018

The array of 118 altitudes z_i, measured densities ρ_i and fractional statistical uncertainties Δ_i given in Table 2.4 are the input data for the least square mathematical procedure described in Section 2.2.2.

2.2.4 Results of Analytical Fit for April 23, 1976 Low Background Betasonde Flight

By use of the data in Table 2.4 for z_i, ρ_i and Δ_i, the least square procedure was applied for $j_m = 2 - 5$ to obtain the values for the coefficients A_j. For each set of solutions, the results for rms sum of the weighted deviations between the analytical fit and experimental points Δ was determined. This is the quantity that was minimized to produce the solution obtained. Δc, the rms unweighted deviation sum, was also calculated from (2.14); both Δ and Δc are to be compared to Δm, the rms fractional uncertainty, from (2.12). Results for all of these parameters, along, with ρ_o from (2.17), are given in Table 2.5.

The rms fractional uncertainty, Δm, is independent of j_m and has the value 0.039. As noted above, a satisfactory fit is one in which the difference between Δc and Δm is acceptably small.

Model fitting often requires use of 10 to 14 coefficients in a similar procedure to obtain what is considered to be an adequate fit. Here, we found that for the particular experimental data used, 4 or 5 are sufficient to provide a fit whose accuracy is consistent with the accuracy of the data. Thus, as seen from the table, Δ decreases rapidly as j_m goes from 2 to 3, but with j_m as large as 5, the accuracy of the fit is marginally better. Δc appears to go through a minimum at $j_m = 4$. As observed above, a fit derived by minimizing Δ, the rms sum of the deviations weighted inversely with the uncertainties, is taken here as the proper procedure to follow. This causes those points with most accuracy to produce the most effect on the fit. However, such a fit should not be allowed to produce a large value of Δc, the rms sum of the unweighted deviations. In view of the fact that there is undoubtedly some short-term atmospheric variability in density, it is unlikely that a fit in which Δc approaches Δm much more closely than in the present case would be expected. Thus, in the present instance at least, a criterion for selecting the most satisfactory of the fits obtained by minimizing Δ, is that particular one for which Δc is a minimum; $j_m = 4$ here. Whether such a dependence on j_m will always occur is not presently known. When the results of additional flights are available, futher investigation of the method of selecting the optimum fit should be made.

Table 2.5 Parametric Results of Analytical Fit
for LBB Flight on April 23, 1976

Δ_m = .03909, z_o = 26.2 km

j_m	A_1	A_2	A_3	A_4	A_5	$\rho_o(g/m^3)$	Δ	Δ_c
2	-.35136+1	+.15248+0	-	-	-	33.568	.05709	.21408
3	-.35771+1	+.17100+0	-.84900-3	-	-	35.770	.03723	.04505
4	-.35753+1	+.17017+0	-.76747-3	-.18776-5	-	35.707	.03722	.04475
5	-.35864+1	+.17821+0	-.21034-2	+.69676-4	-.11369-5	36.104	.03675	.04921

Read $N\pm n$ as $N \times 10^{\pm n}$ for all A_j

Summed over entire altitude range:

Δ_m = RMS fractional statistical uncertainty in measured density, Eq. (3.6).

Δ = RMS value of approximate difference D_i between measured and fit-calculated densities, weighted inversely with fractional statistical uncertainty in measured density.

Δ_c = RMS value of actual difference D_i [Eq. (2.11)] between measured and fit-calculated densities, unweighted, Eq. (2.14).

The quantity $\bar{H}(z)$ given by (2.18) is actually to be used in (2.10) to provide the optimum analytical fit to the data. However, for purposes of comparison with models it is useful to have the value of H(z). This can be determined as follows. Note from (2.9) that

$$H(z) = -1\Big/\left(\frac{d\rho/\rho}{dz}\right) \tag{2.19}$$

But, from (2.10) for the fit used here this gives

$$H(z) = 1\Big/\frac{d}{dz}\left(\frac{z - z_0}{\bar{H}(z)}\right) \tag{2.20}$$

Use of (2.18) then yields

$$H(z) = 1\Big/\sum_{j=2}^{j_m} A_j (j-1)(z-z_0)^{j-2} \tag{2.21}$$

Consequently, once the A_j have been determined it is possible to calculate the value of H(z) as well as $\bar{H}(z)$.

For the fit with $j_m = 4$, results are given in Table 2.6 and Figures 2.2 and 2.3. The first three columns of the table give z_i, ρ_i and $\Delta\rho_i$ (ALT, DENSITY and UNC in Table 2.4). The next three give $\rho(z)$, $\bar{H}(z)$, and H(z) as calculated from (2.10), (2.18), and (2.21), respectively. The next column gives the fractional difference between measured ρ_i and calculated $\rho(z)$. The final column, labeled RMS FRAC, is a running rms average of the fractional difference for that altitude with that of the four previous (higher altitude points). Hence, it is assigned the value zero for the four highest altitude points.

Examination of the variation of RMS FRAC with altitude shows those regions in which the best fit is obtained. At the highest altitudes the average difference for any single point is as high as 7-8%, due to the small number of counts recorded there. As the sonde descends it goes through a region where the average difference is on the order of 2%. There is, however, a lower altitude region (below about 20 km) in which beta particle energy loss dominates the effects of scattering, and the count rate decreases as z decreases (Ref. 1.3). Thus, near 20 km there is little variation of count rate with z, and the density uncertainty becomes very large in spite of the large count rates. This region is being approached

Table 2.6 Altitude Dependence Results of Analytical Fit for LBB Flight on April 23, 1975

$j_m = 4$

RESULTS OF FIT

J	A(J)
1	-0.35753E+01
2	0.17017E+00
3	-0.76747E-03
4	-0.18776E-05

Z0= 26.2 KM
RHO0= 35.707 G/M**3

RMS FRAC=RMS AVG OF PREV 5 DIFF FRACS

ALT KM	RHO-MEAS G/M**3	UNCER G/M**3	RHO-CALC G/M**3	HBAR(Z) KM	H(Z) KM	DIFF FRAC	RMS FRAC
64.0	0.168	0.019	0.190	7.221	9.606	-0.117	0.000
64.3	0.198	0.021	0.184	7.236	9.661	0.073	0.000
64.2	0.182	0.020	0.186	7.231	9.642	-0.024	0.000
63.5	0.185	0.020	0.201	7.198	9.516	-0.077	0.000
62.9	0.232	0.023	0.214	7.170	9.412	0.086	0.081
62.1	0.225	0.023	0.233	7.133	9.276	-0.033	0.064
61.0	0.291	0.026	0.262	7.083	9.096	0.109	0.073
60.0	0.298	0.026	0.293	7.038	8.940	0.017	0.073
59.1	0.357	0.029	0.324	6.998	8.805	0.100	0.078
57.9	0.355	0.028	0.372	6.947	8.632	-0.046	0.071
55.9	0.504	0.034	0.471	6.862	8.360	0.070	0.077
54.9	0.553	0.036	0.532	6.821	8.232	0.040	0.062
53.9	0.597	0.037	0.601	6.781	8.108	-0.006	0.061
53.0	0.644	0.038	0.672	6.745	8.001	-0.041	0.046
52.0	0.839	0.044	0.762	6.706	7.885	0.101	0.061
51.2	0.854	0.044	0.844	6.675	7.796	0.012	0.052
50.5	0.889	0.046	0.923	6.648	7.719	-0.037	0.052
50.0	0.897	0.051	0.985	6.629	7.666	-0.090	0.066
49.5	1.069	0.056	1.052	6.611	7.613	0.016	0.063
48.6	1.290	0.055	1.185	6.577	7.521	0.089	0.060
48.1	1.191	0.053	1.267	6.559	7.471	-0.060	0.065
47.7	1.316	0.055	1.337	6.544	7.431	-0.015	0.063
47.2	1.388	0.064	1.430	6.526	7.383	-0.029	0.051
46.8	1.443	0.065	1.510	6.512	7.344	-0.044	0.054
46.4	1.437	0.064	1.594	6.498	7.306	-0.099	0.057
45.3	1.835	0.104	1.731	6.476	7.250	0.060	0.057
45.3	1.945	0.075	1.855	6.459	7.205	0.048	0.061
45.0	1.871	0.074	1.935	6.448	7.178	-0.033	0.061
44.2	2.044	0.075	2.164	6.421	7.106	-0.055	0.063
43.9	2.239	0.079	2.257	6.410	7.080	-0.008	0.045
43.4	2.510	0.076	2.423	6.393	7.037	0.036	0.040
43.1	2.322	0.072	2.529	6.383	7.012	-0.082	0.049

Table 2.6 (cont'd)

ALT KM	RHO-MEAS G/M**3	UNCER G/M**3	RHO-CALC G/M**3	HBAR(Z) KM	H(Z) KM	DIFF FRAC	RMS FRAC
42.8	2.622	0.078	2.639	6.373	6.986	-0.007	0.047
42.5	2.699	0.079	2.755	6.363	6.961	-0.021	0.041
42.2	2.821	0.080	2.877	6.353	6.936	-0.019	0.042
41.9	2.831	0.091	3.004	6.343	6.912	-0.058	0.047
41.7	3.086	0.095	3.093	6.336	6.895	-0.002	0.029
41.1	3.410	0.091	3.375	6.316	6.847	0.010	0.029
40.8	3.499	0.092	3.526	6.307	6.823	-0.008	0.028
40.5	3.671	0.095	3.685	6.297	6.800	-0.004	0.027
40.2	3.666	0.094	3.852	6.287	6.776	-0.048	0.022
40.0	3.931	0.098	3.967	6.281	6.761	-0.009	0.023
39.7	4.042	0.103	4.148	6.271	6.738	-0.025	0.025
39.5	4.285	0.106	4.273	6.264	6.722	0.003	0.025
39.3	4.451	0.108	4.402	6.258	6.707	0.011	0.025
39.0	4.671	0.123	4.604	6.248	6.684	0.015	0.015
38.5	4.768	0.123	4.962	6.233	6.647	-0.039	0.022
38.3	5.008	0.114	5.114	6.226	6.632	-0.021	0.021
38.1	5.225	0.116	5.271	6.220	6.618	-0.009	0.022
37.9	5.618	0.120	5.433	6.214	6.603	0.034	0.026
37.6	5.654	0.120	5.685	6.204	6.582	-0.006	0.025
37.4	5.916	0.123	5.861	6.198	6.567	0.009	0.019
37.2	6.054	0.122	6.043	6.192	6.553	0.002	0.017
37.0	6.096	0.123	6.230	6.186	6.539	-0.022	0.019
36.8	6.498	0.128	6.424	6.180	6.525	0.012	0.012
36.2	7.242	0.136	7.045	6.161	6.483	0.028	0.017
36.1	7.693	0.141	7.154	6.158	6.476	0.075	0.038
35.9	7.725	0.141	7.379	6.152	6.462	0.047	0.043
35.7	7.478	0.139	7.611	6.146	6.448	-0.017	0.043
35.5	8.097	0.145	7.851	6.140	6.435	0.031	0.045
35.4	8.086	0.145	7.974	6.137	6.428	0.014	0.043
35.2	8.286	0.147	8.226	6.131	6.414	0.007	0.027
35.1	8.819	0.153	8.356	6.128	6.408	0.055	0.030
34.9	8.743	0.170	8.621	6.122	6.394	0.014	0.030
34.5	9.226	0.156	9.179	6.110	6.368	0.005	0.027
34.4	9.692	0.163	9.324	6.107	6.361	0.039	0.031
34.3	9.388	0.159	9.472	6.104	6.355	-0.009	0.031
34.1	9.123	0.156	9.775	6.098	6.341	-0.067	0.036
34.0	9.811	0.164	9.930	6.095	6.335	-0.012	0.035
33.9	10.267	0.171	10.088	6.092	6.328	0.018	0.036
33.7	10.332	0.172	10.413	6.086	6.315	-0.008	0.032
33.6	11.012	0.177	10.579	6.083	6.309	0.041	0.036
33.5	11.227	0.199	10.748	6.080	6.303	0.045	0.029
33.1	11.205	0.178	11.454	6.068	6.277	-0.022	0.030
33.0	11.360	0.177	11.638	6.066	6.271	-0.024	0.031
32.9	12.070	0.184	11.825	6.063	6.264	0.021	0.032
32.8	12.084	0.184	12.015	6.060	6.258	0.006	0.026
32.6	12.810	0.189	12.406	6.054	6.245	0.033	0.023

Table 2.6 (cont'd)

ALT KM	RHO-MEAS G/M**3	UNCER G/M**3	RHO-CALC G/M**3	HBAR(Z) KM	H(Z) KM	DIFF FRAC	RMS FRAC
32.4	13.332	0.192	12.810	6.048	6.233	0.041	0.027
32.2	13.400	0.192	13.228	6.042	6.221	0.013	0.026
32.1	13.876	0.195	13.443	6.039	6.214	0.032	0.028
32.0	13.995	0.219	13.661	6.037	6.208	0.024	0.030
31.6	14.413	0.195	14.572	6.025	6.184	-0.011	0.027
31.5	15.439	0.206	14.810	6.022	6.178	0.043	0.027
31.3	14.947	0.199	15.297	6.017	6.165	-0.023	0.029
31.2	15.153	0.203	15.548	6.014	6.159	-0.025	0.027
31.0	15.627	0.208	16.061	6.008	6.147	-0.027	0.028
30.8	16.701	0.221	16.593	6.002	6.135	0.007	0.027
30.7	16.723	0.221	16.866	6.000	6.129	-0.008	0.020
30.5	17.451	0.227	17.426	5.994	6.117	0.001	0.017
30.4	17.518	0.255	17.713	5.991	6.112	-0.011	0.014
30.0	19.096	0.243	18.914	5.980	6.088	0.010	0.008
29.9	19.421	0.253	19.227	5.977	6.082	0.010	0.009
29.7	19.072	0.243	19.870	5.972	6.071	-0.040	0.020
29.6	19.144	0.245	20.200	5.969	6.065	-0.052	0.031
29.5	19.605	0.258	20.536	5.966	6.059	-0.045	0.036
29.3	20.929	0.296	21.226	5.960	6.047	-0.014	0.037
29.1	20.666	0.283	21.941	5.955	6.036	-0.058	0.045
29.0	20.896	0.294	22.307	5.952	6.030	-0.063	0.050
28.9	23.378	0.444	22.681	5.949	6.025	0.031	0.046
28.6	21.589	0.327	23.840	5.941	6.008	-0.094	0.059
28.5	23.648	0.400	24.241	5.938	6.002	-0.024	0.060
28.3	24.303	0.439	25.063	5.933	5.991	-0.030	0.055
28.2	25.138	0.437	25.485	5.930	5.985	-0.014	0.048
28.1	26.962	0.433	25.914	5.927	5.980	0.040	0.050
27.9	27.242	0.445	26.797	5.922	5.969	0.017	0.027
27.7	28.263	0.498	27.711	5.917	5.957	0.020	0.026
27.6	27.341	0.449	28.180	5.914	5.952	-0.030	0.026
27.4	30.125	0.599	29.144	5.909	5.941	0.034	0.029
27.2	32.794	0.599	30.143	5.903	5.930	0.088	0.046
27.1	30.542	0.609	30.655	5.900	5.925	-0.004	0.045
27.0	32.576	0.598	31.178	5.898	5.919	0.045	0.049
26.9	31.091	0.558	31.709	5.895	5.914	-0.019	0.047
26.7	35.629	0.632	32.801	5.890	5.903	0.086	0.059
26.6	35.194	0.620	33.361	5.887	5.898	0.055	0.051
26.5	32.020	0.588	33.932	5.884	5.892	-0.056	0.057
26.3	37.662	0.671	35.105	5.879	5.882	0.073	0.062
26.2	37.429	0.669	35.707	5.876	5.876	0.048	0.065

TOT. RMS FRAC. RHOMEAS-RHOCALC DIFF= 0.04475
TOT. RMS FRAC. RHOMEAS. UNCERTAINTY= 0.03909

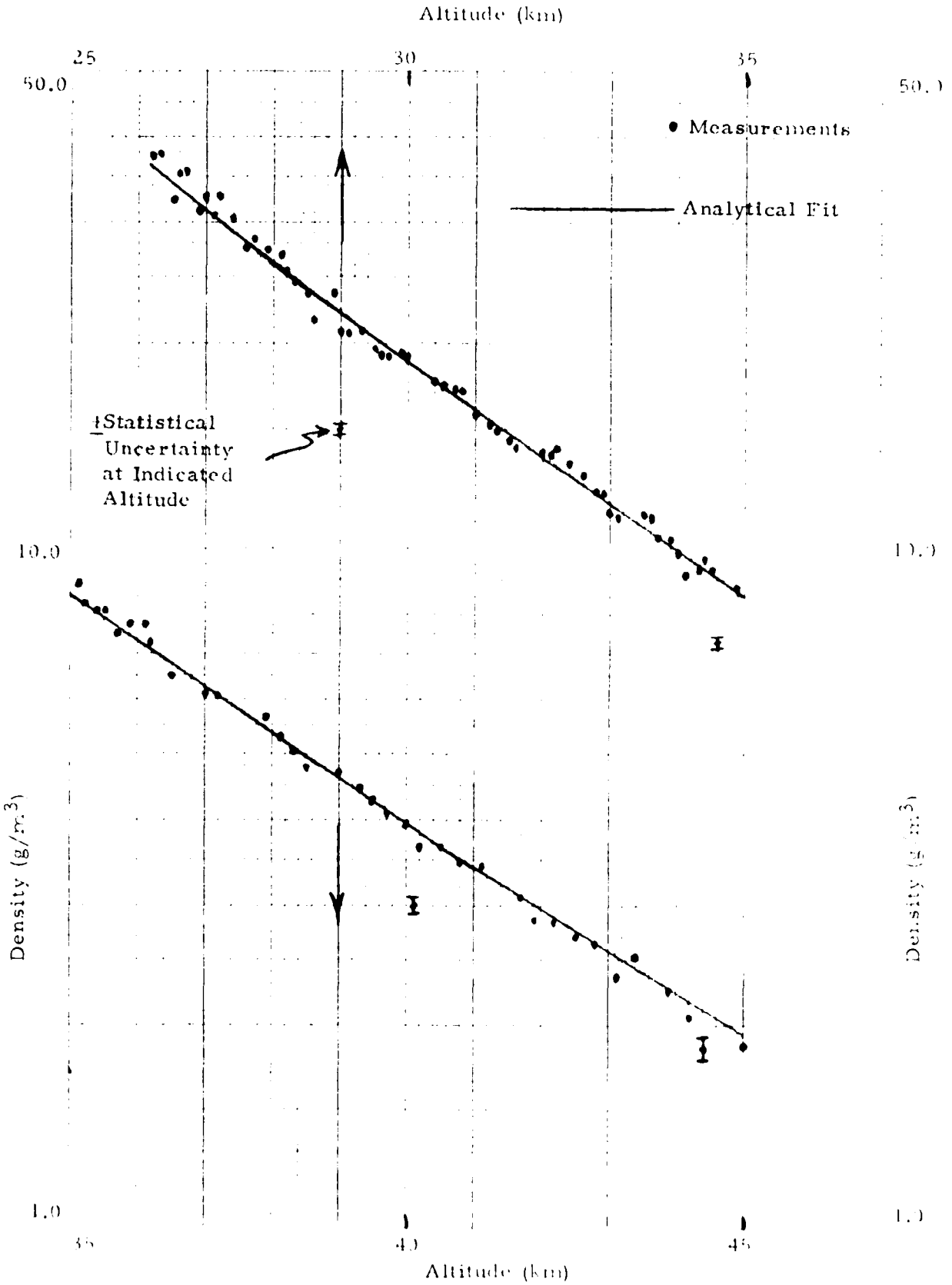

Fig. 2.2 Low Background Betasonde Air Density Results for Flight at White Sands Missile Range on 4/23/76, 25-45 km.

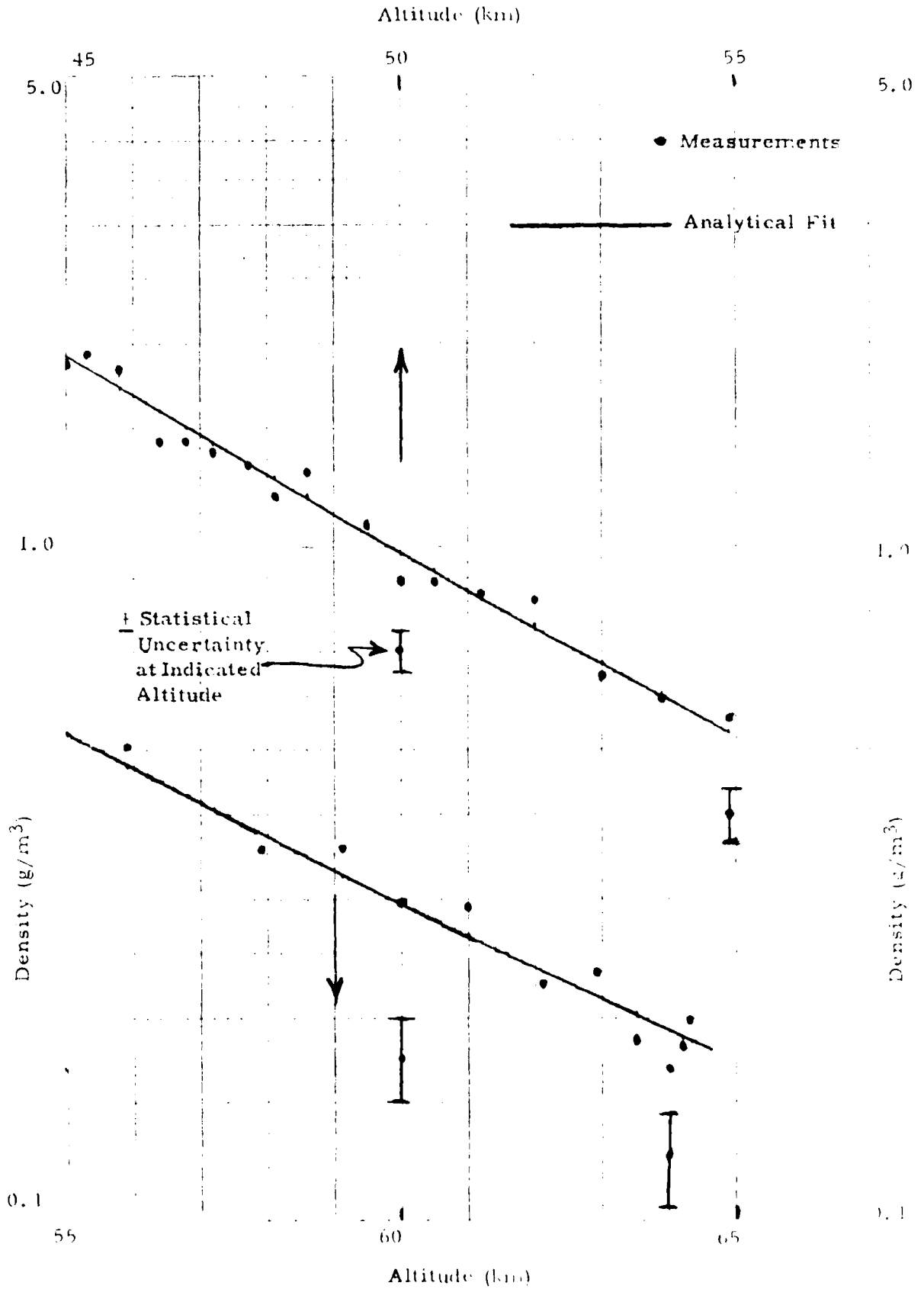

Fig. 2.3 Low Background Betasonde Air Density Results for Flight at White Sands Missile Range on 4/23/70, 45-65 Km.

at the lowest altitudes in Table 2.6, which accounts for much of the average difference of about 5% there. As noted previously, the 4 measurements made in the vicinity of the 64 km apogee during a period of about 20 seconds are particularly important, since the sonde descends rapidly for some distance thereafter. The data from these four points could have been averaged together to give one measurement at the average altitude of 64.0 km. The result would have been 0.1833 g/m^3 with a fractional uncertainty of .054 (about half that of each of the four points). The calculated result from the fit is .190 g/m^3, a fractional difference of only .035. Thus, these four points, as utilized with least square procedure, serve to define $\rho(z)$ accurately in the apogee altitude region.

It is of interest to compare the H(z) values with those of an appropriate model atmosphere, such as that of the Spring/Fall Mid-Latitude Model (Ref. 2.4). Values of H(z) are not given in that particular model. It is straightforward, however, to derive the associated H(z) by fitting the two $\rho(z)$ values that bracket the altitude of interest. By use of this procedure and the results of Table 2.6 we obtain the following:

Table 2.7

Comparison of Scale Heights
for 4/23/76 Flight

z(km)	H_{model}(km)	H_{fit}(km)
25	6.35	~5.85
30	6.50	6.09
35	6.47	6.40
40	6.85	6.76
45	7.24	7.18
50	8.04	7.67
55	8.40	8.24
60	8.11	8.94
65	8.08	~9.70

In general the H(z) values from the analytical fit are slightly below those of the model in the 25-30 km region, close in the 35-55 km region, and somewhat higher in the 60-65 km region. Certainly, the agreement is very reasonable on the average.

2.2.5 Discussion

In summary, we believe that the results of applying the least square mathematical procedure developed in Section 2.2.2 to the LBB flight data in Section 2.2.3 show the procedure to be valid. An accurate analytical fit was obtained that is capable of representing the entire tabular array of data, and we believe that the procedure should be applied to future LBB or Beta-sonde II flights.

It should be observed that a similar procedure can also be applied to other altitude-dependent measurements, for example temperature and pressure, provided a tabular array of the measured quantity, and its uncertainty, is available. In the case of pressure measurements the above procedure could be used almost in its exact form, since pressure also depends exponentially on altitude. For temperature the analytical function would have to be chosen to represent, in an average manner, the known variation of that quantity with altitude.

3. BETASONDE II DESIGN AND OPERATION

In this section the design of the advanced model, Betasonde II, is given, and details of the unit, as fabricated, are presented. Betasonde II is presently available for flight and could readily be fitted into rockets other than the Arcas.

3.1 Description

A photograph of the completed sonde, which was originally designed for flight on an Arcas rocket, is shown in Fig. 3.1. The basic configuration is given in Fig. 3.2. A tripod-supported boom carries the annular beta source which irradiates the air volume in the region between source and detector, outside the shield. The forward-scattered beta rays are detected by a surface barrier type semiconductor detector located at the base of the tripod. A shield is placed between the source and detector to prevent direct passage of beta particles from the source to the detector. A plastic disc is placed on the side of the shield that faces the source, in order to reduce bremsstrahlung generation. The distances of the source to the detector and to the shield are fixed for optimum system response characteristics. Work to optimize that response was carried out during the development phase of this contract and is contained in our report: Atmospheric Density Measurement In The Middle Atmosphere (Ref. 1.1).

The original concept of the high-altitude Betasonde utilized an annular surface barrier detector with the source boom mounted through the center of that detector. Although this arrangement has the advantage of simpler mechanical construction, it has been found that the cost of a ruggedized, light weight, annular detector outweighs these advantages. The choice of the below described non-annular detector is based on its cost effectiveness and on the manufacturer's experience with the construction of such a special detector.

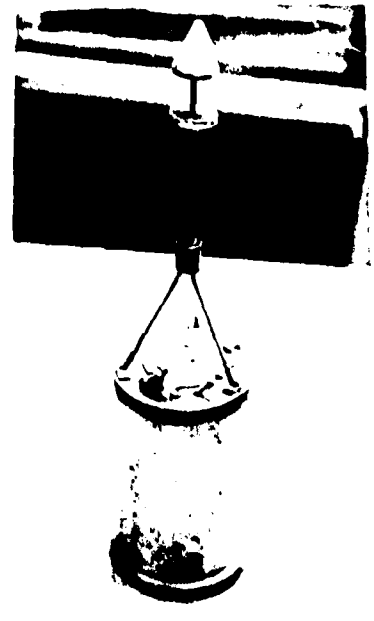

Fig. 3.1 Photograph of Completed Betasonde II Atmospheric Density Sonde

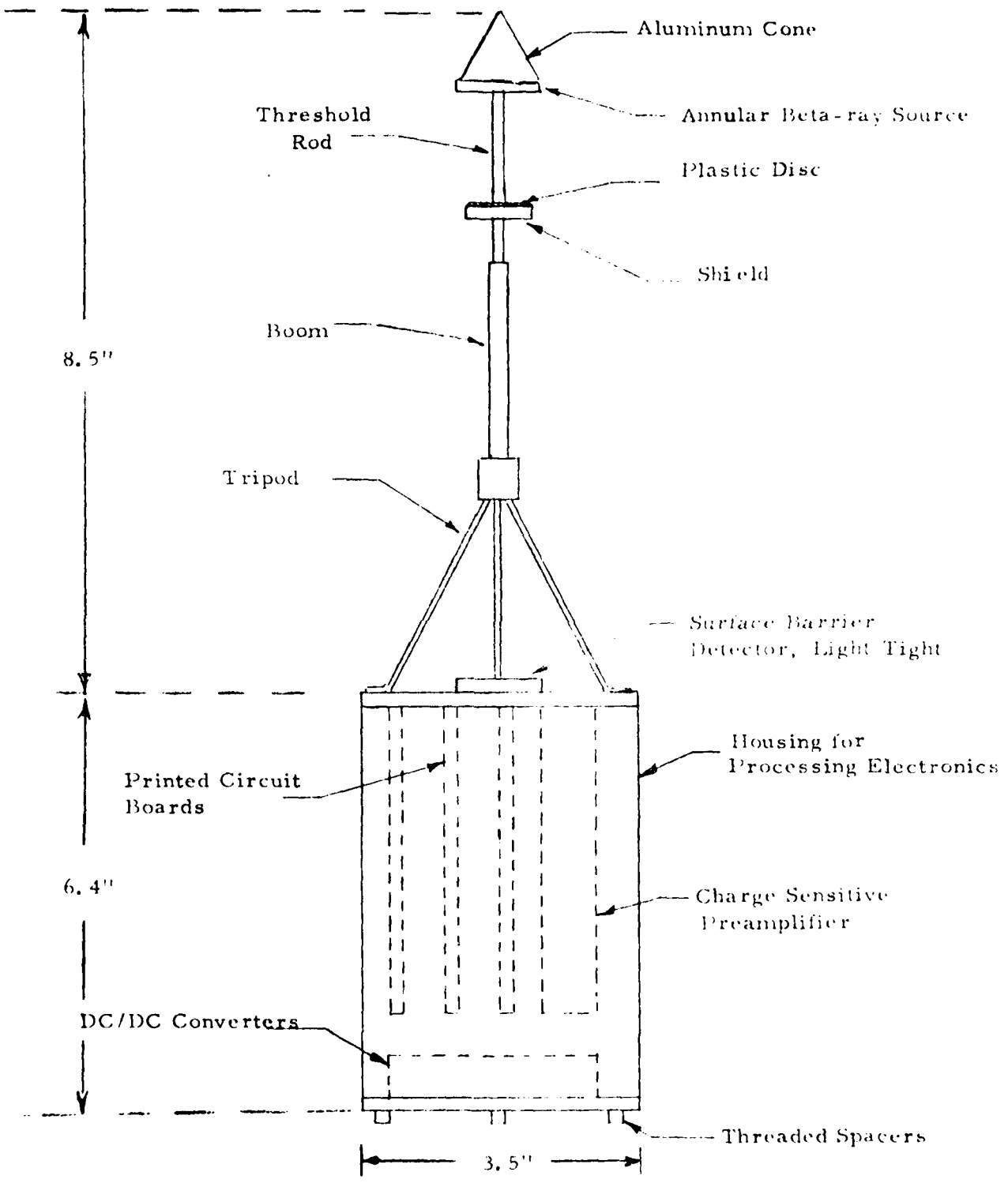

Figure 3.2 Betasonde II - Simplified View of Overall Configuration.

The detector is a ruggedized surface barrier type with an active area of 450 mm^2, sufficient to give a reasonable count rate up to an altitude of 80 km.* Since a standard detector inherently responds to light in the visible spectrum, it is necessary for this application to have a specially processed detector featuring a light-tight front surface. According to the manufacturer (Ortec, Inc.) a light-tight front surface can be obtained with 120$\mu g/cm^2$ of aluminum, which is vapor deposted directly on the detector material. The latter is p-type silicon (rather than the standard n-type) in order for the aluminum to become the rectifying contact of the surface barrier diode, and thus the front of the detector. Other features of the detector are low noise (18 keV max for beta particles) and a depletion depth of 300μm at a bias of 100V. The relatively low bias voltage is a desirable feature, simplifying the design and assuring low power dissipation of the bias voltage supply.

The source consists of an annular disc with the radioisotope (Pm-147) deposited and sealed on the underside of it. The center hole of the disc is tapped for convenient mounting to the boom. A cone fabricated from aluminum serves as a protective cover and firmly holds the source in place. Source intensity is of the order of 500 mCi for 80 km maximum altitude.

The lower portion of the sonde contains all necessary electronics to process the signals from the detector and to supply the required power for the electronics as well as the detector. The system circuitry is housed in a cylindrical container, constructed of aluminum with a diameter of 3-1/2 in. by 6-3/8 in. long. The charge sensitive preamplifier (CSPA) is additionally shielded by its own housing to protect it from electro-magnetic interference. The rest of the electronics is mounted on three printed circuit boards which individually plug into a motherboard. The internal power supplies (DC/DC converters) are mounted to the bottom cover for improved heat transfer to the outside environment.

The telemetry antenna, not shown in Fig. 3.1, may be attached to the boom and along one leg of the tripod. Grommets in the top and bottom of the electronics housing are provided for a coaxial antenna feed line which would pass through the housing. The mechanical interface of the rocket telemetry section and the sonde simply consists of four threaded spacers used to bolt the two units together. Electrically the two units are hard-wired together.

3.2 Operation

The electronic system of the sonde is illustrated in block diagram form in Fig. 3.3. The instrument consists essentially of a solid state detector/amplifier/threshold discriminator chain driving selectively a binary divider or passing right through to be applied to telemetry (TM) after suitable shaping and multiplexing with detector temperature information.

---

*This is for a 500 mCi source intensity.

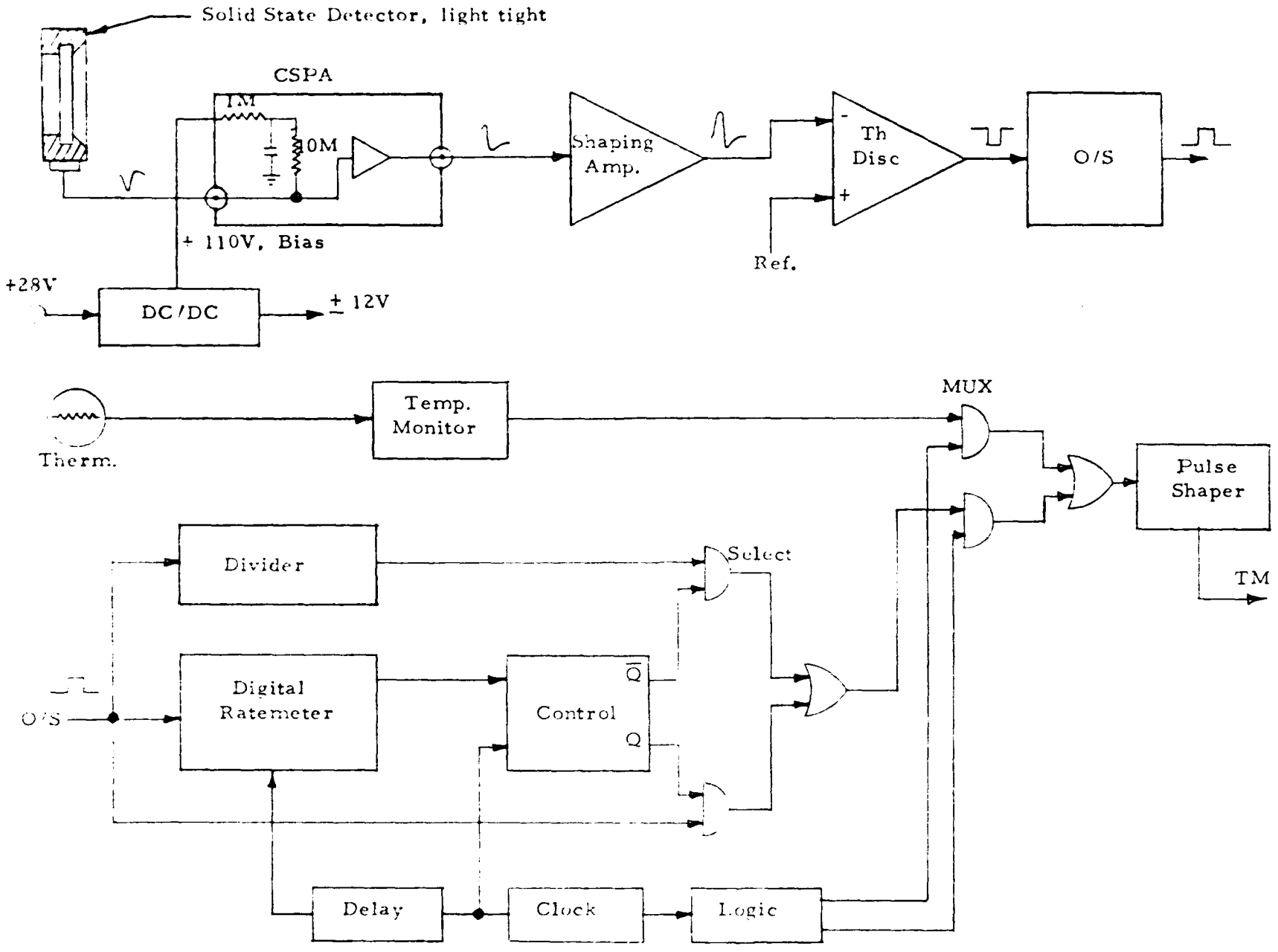

Fig. 3.3 Betasonde II - Block Diagram of Electronics.

The two signals (pulses or temperature) are alternately applied to TM by means of the multiplexer. A more detailed description of the system is given below.

The forward-scattered beta rays incident on the solid state detector produce hole-electron pairs in the silicon detector (1 hole-electron for each 2.3 eV of deposited energy) which are swept up by the electric field created by the bias voltage, resulting in a charge pulse proportional to the incident deposited energy at the detector output. Overbiasing the solid state detector to +110V assures that it is totally depleted and will remain so under varying ambient conditions; and all charge will be collected.

The charge pulse is converted to a voltage pulse by the charge sensitive preamplifier (CSPA) and is then amplified and shaped by the shaping amplifiers. Double differentiation/double integration shaping is used for near optimum signal to noise ratio. Use of a charge sensitivie preamplifier assures that the shaping amplifier output conversion gain of 4 volts per MeV of deposited energy will be insensitive to variation in solid state detector or stray capacitances.

An output pulse is produced by the threshold discriminator (Th. Disc.) each time the shaping output level exceeds the fixed reference level. This reference is set at a voltage equivalent to about 2.5 times the energy noise level of the detector. As stated above, the maximum FWHM noise output from the detector is 18 keV - including electronics noise - which results in an energy threshold level of 45 keV. The discriminator pulses are standardized as to pulse width and height with a monostable multivibrator or One-Shot (O/S).

The One-Shot output pulses are simultaneously applied to a binary Divider ($\div 8$), an OR gate (Select) and a Digital Ratemeter. As long as the O/S pulse rate does not exceed about 10 keps the O/S pulses are directly output to the TM via the OR gate to give the desired air density information. If the count rate exceeds about 10 keps, the output is selected from the $\div 8$ circuit, thus extending the maximum possible input counting rate by a factor of 8. The selection process is based on the ratemeter output and its associated control and logic circuits. The state of the ratemeter output is continuously sampled. When the input count rate exceeds 10,240 cps the output goes low and the control circuit selects the $\div 8$ output as the air density information channel for TM. Below that count rate threshold the O/S pulses are directly routed to TM via the Select gate. The Clock and Delay circuits associated with the Ratemeter and Control provide the necessary logic signals for the sampling operation and furnish a time base for the Ratemeter.

The temperature of the solid state detector is continuously measured with a small thermistor bead in contact with the detector housing. The output voltage of the thermistor varies according to temperature in a non-linear fashion and is processed by a voltage to frequency converter in the Temperature Monitor circuit. Full scale output is 200 Hz at +50°C non-linearly

decreasing to about 40 Hz at -10°C. This range gives ample margin for the expected temperature extremes of 0° to +45°C derived from measurements of other payloads flown on Arcas rockets. The range also covers the upper operating temperature limit of the detector of 45°C.

Since the TM transmitter can only handle one information channel, the selected pulse output and the Temperature Monitor output are multiplexed. Time allocation is: 50 seconds for pulse output, 5 seconds for temperature output. The FM/FM transmitter can process signal rates of up to 10 kHz. To achieve sufficient bandwidth for a pulse output, a dead time circuit in the Pulse Shaper limits the pulse repetition rate to 5 kHz. Since the sonde input pulse rate can exceed that rate, up to 10 kHz, a dead time correction must be applied as described in the annual report (Ref. 1.1). Also included in the Pulse Shaper is a level translator converting standard logic pulses to a 0 to -12V pulse of 40μs duration. This makes the output compatible with FM/FM transmitters previously flown on Arcas rockets.

All necessary power for the system is derived from 2 DC/DC converters connected to the +28V battery pack of the TM section. The low voltage converter delivers $\pm$12V at +22 ma and -16 ma, respectively. The H. V. converter delivers +110V at max 4 ma. The power requirement for the battery is 28V at 120 ma for the above output power.

For completeness, the detailed schematics of the various circuits of the block diagram are included in this report, and are contained in Figs. 3.4 thru 3.7. These show the as-constructed circuits contained in the completed sonde in Figs. 3.1 thru 3.3.

3.3 Prometheum Radiation Source

A Pm-147 source of intensity 500 mCi was ordered from Isotope Products Labs in October, 1977. When received, however, our measurements indicated an actual emission less than 100 mCi. It was returned to IPL for possible repair, but when returned, it was of the same intensity. Thus, all measurements reported above were made with the older Pm-147 source, which had an emission near 100 mCi when used. We believe it likely that the specific activity of the isotope used to prepare the IPL source was not as high as necessary. We feel certain that a source with > 500 mCi Pm-147 emission can be fabricated. But it will require more procurement effort and quality assurance than was possible during this limited program.

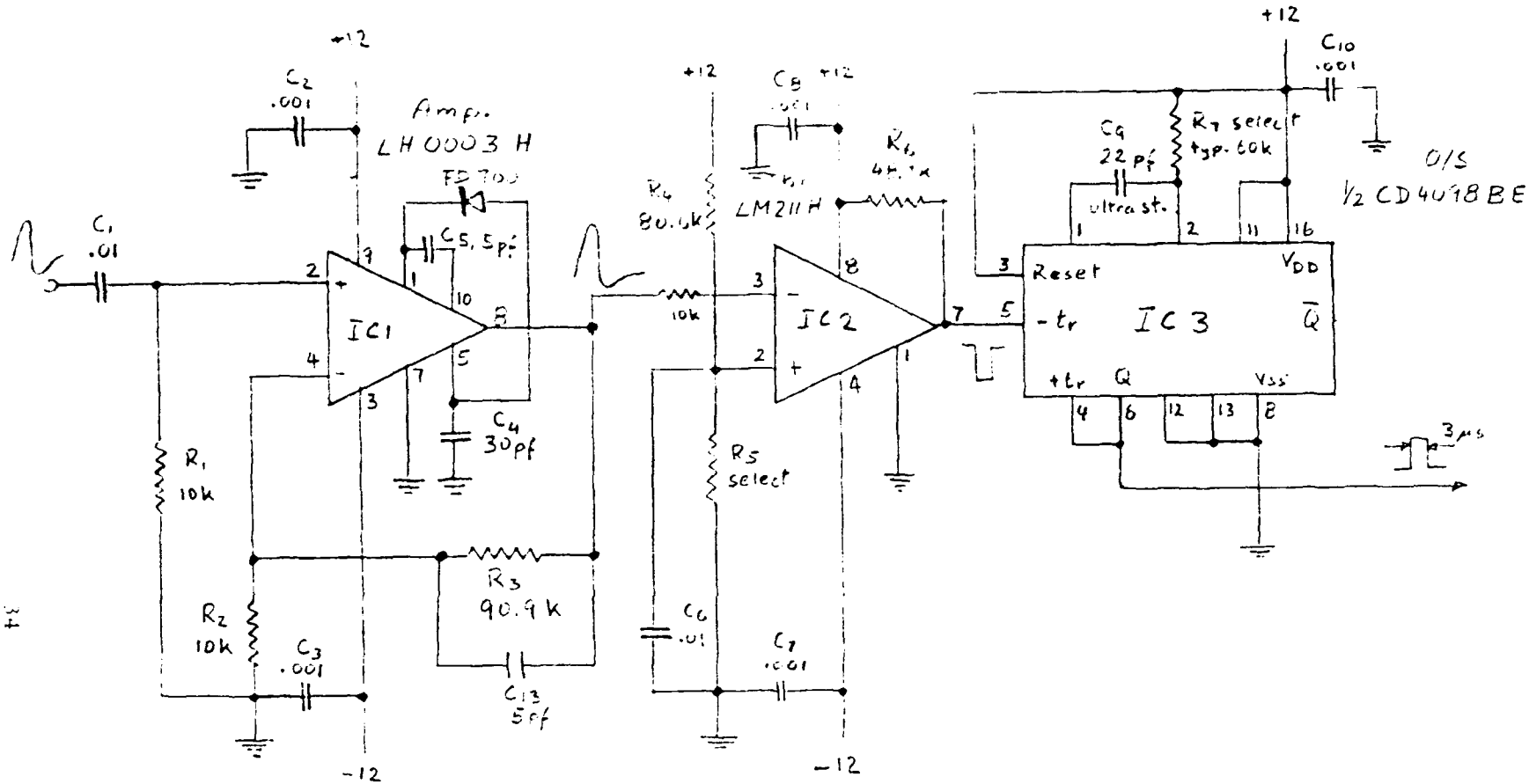

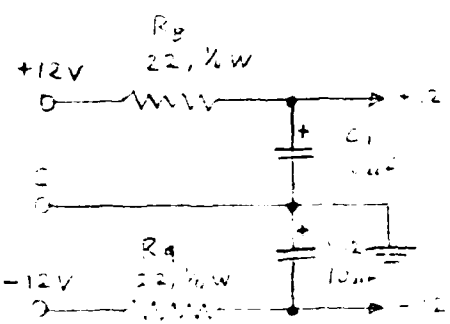

Fig. 3.4 Betasonde II - Schematic, Shaping Amplifier Threshold Discriminator, One-Shot

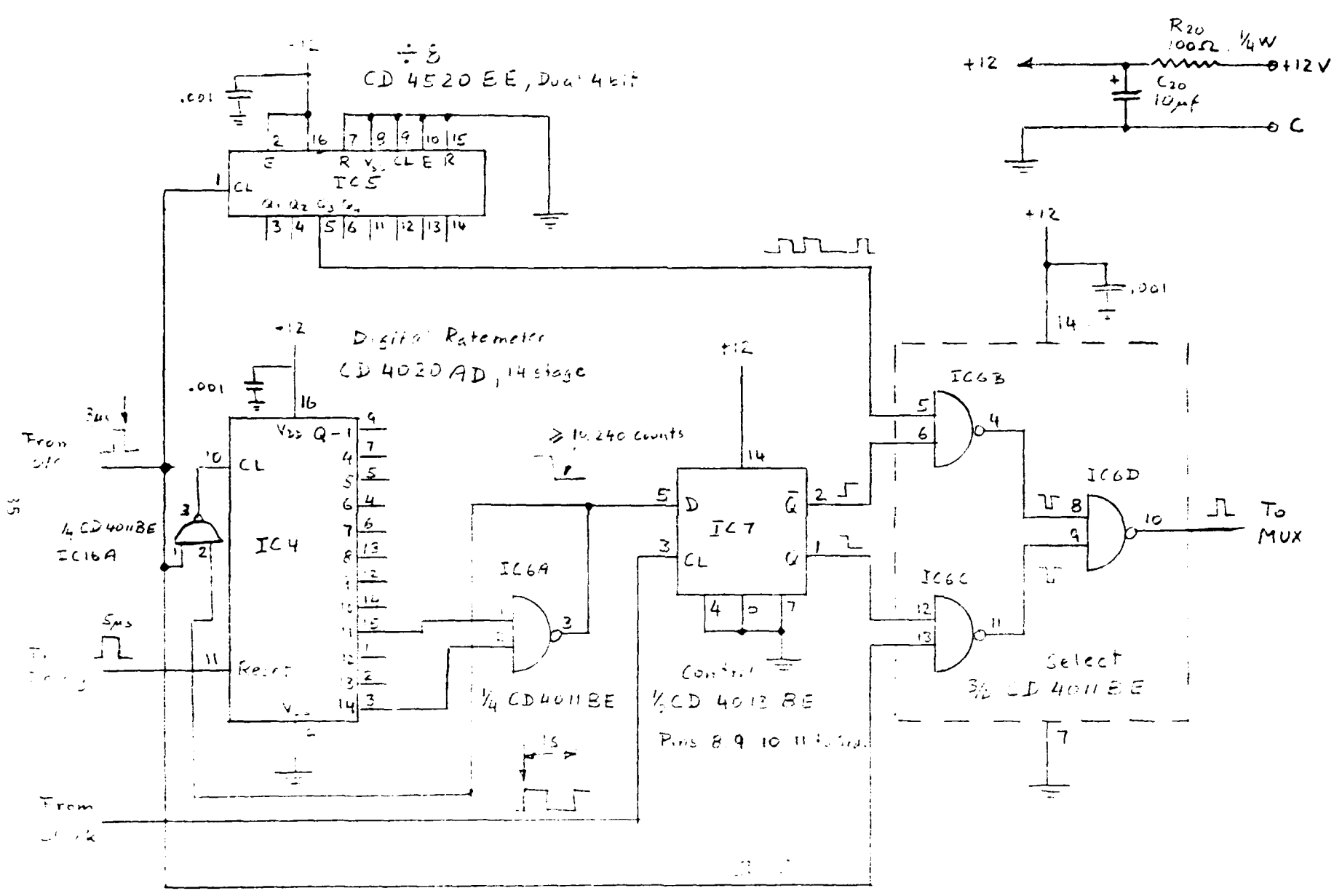

Fig. 3.5 Betasonde II - Schematic, Divider ÷3, Digital Ratemeter Control and Select.

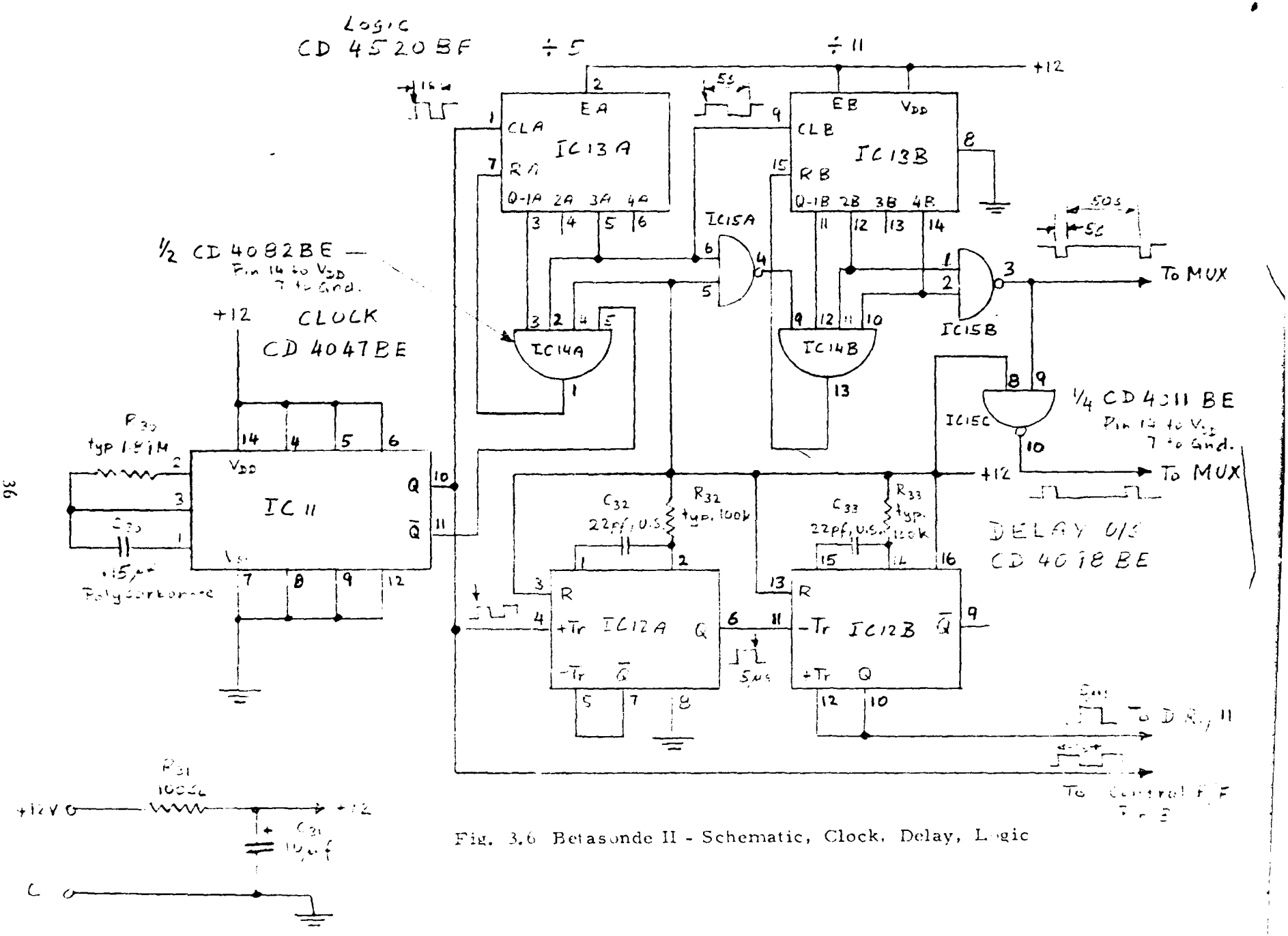

Fig. 3.6 Betasonde II - Schematic, Clock, Delay, Logic

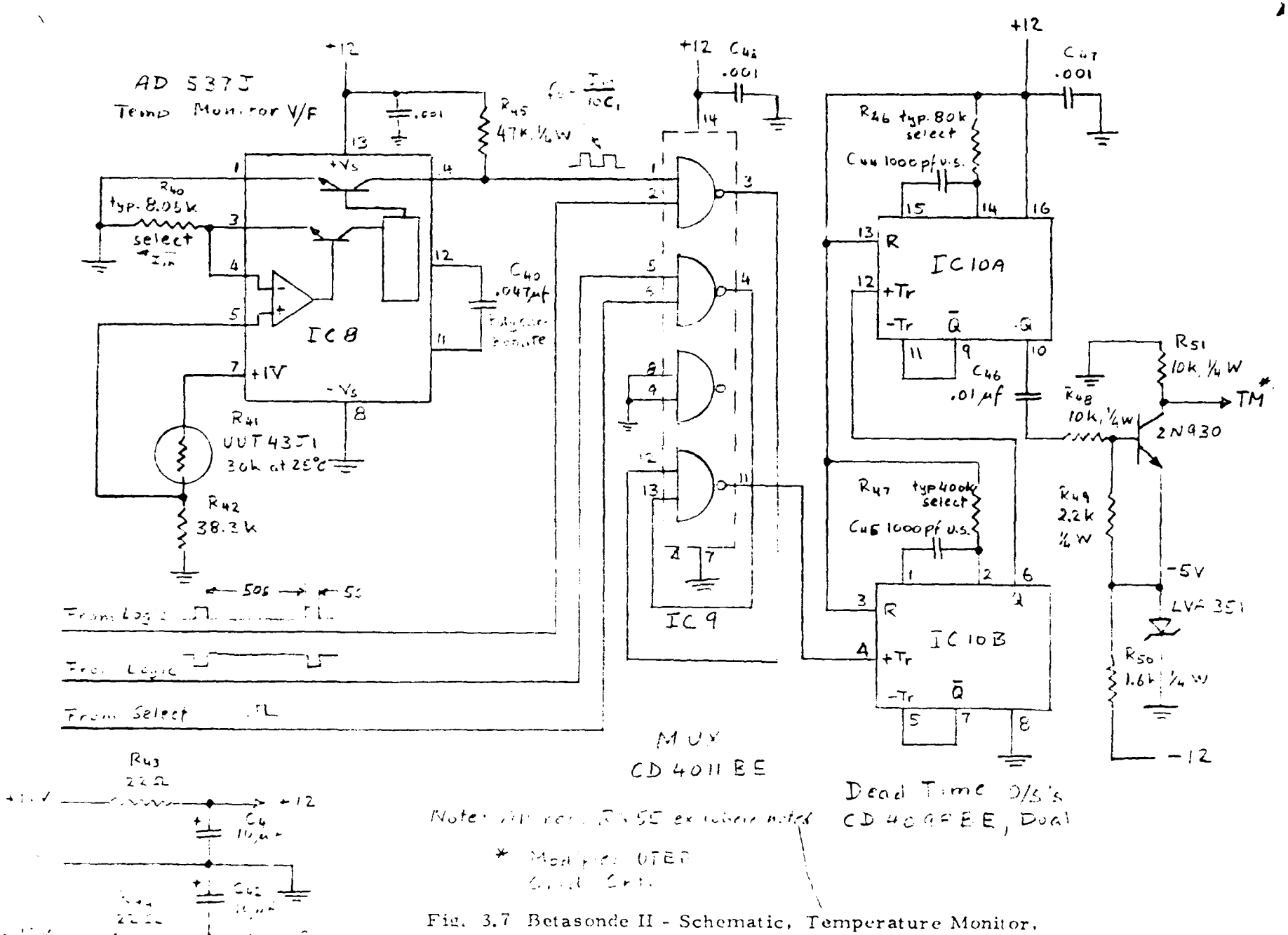

Fig. 3.7 Betasonde II - Schematic, Temperature Monitor, MUX, Pulse Shaper

3.4 Specifications

The pertinent parameters of the Betasonde II atmospheric density sonde are tabulated below:

Altitude Range*	25-65 km
Beta Source*	Pm-147, approx. 100 mCi
Detector	Surface barrier p-type silicon detector, light-tight, 450 mm^2, 300 μm depletion depth.
Telemetry Output	Two multiplexed outputs: Air density pulses out for 50s, detector temp. pulses out for 5s; 4μs pulses, 0 to -12V of 5 kcps max. repetition rate **
Size	3-1/2 in. diameter by 6-3/8 in. long electronics housing with integral boom extending 8-1/2 in. above housing.
Weight	Total 1.87 lbs (850 g)
Power	28V at 120 ma from battery external to betasonde

*The altitude range can be significantly extended upward by use of a more intense beta source. For a 500 mCi source the altitude maximum would be 80-90 km depending upon the trajectory characteristics.

**This implies that if betasonde is used with other than standard Arcas 1680 MHz transmitter, the TM channel used must be capable of 5 kHz maximum transmission. Capability to count the pulses is all that is required, so that some pulse shape distortion by the transmitter can be tolerated.

4. SUMMARY AND CONCLUSIONS

During Phase I, Research and Development, the following was accomplished.

1. A technique was developed for making an analytic fit to an entire array of density versus altitude data on a least-square-basis. The procedure was applied to data from a Low Background Betasonde flight with good results.

2. By use of theoretical calculations and experimental measurements, it was shown that Pm-147 is the optimum choice source for the single-scattering betasonde. This conclusion would be modified if it were possible to reduce the energy threshold (that energy above which all betas are counted), to about 10-20 keV. In that case, Ni-63 would probably be optimum, and the maximum altitude could be above 100 km.

3. A laboratory model of Betasonde II, the semiconductor-detector version, was constructed and calibrated with Pm-147. Although some wall-effect count rate was evident at very low densities (due, apparently, to the open geometry of the detector), it was possible to obtain meaningful calibration data.

4. The calibration data were used to show that with a Pm-147 source of about 500 mCi, it should be possible to obtain about $\pm$ 6% accuracy in the 90 km region for an Arcas launch having apogee near that altitude. Below that altitude the accuracy would be better.

During Phase II, Design and Fabrication, the following was accomplished.

1. The design of the electronics circuitry was completed. This includes the preamplifier, analog processing, digital logic, timing and output pulse shaping circuitry. The total power requirement was determined as given in the Specifications, Section 3.

2. Breadboards of all circuits were constructed in order to verify the design requirements and goals over the expected temperature range.

3. The procurement of the annular Pm-147 source from Isotope Products Labs was prepared and was confirmed on October 17, 1977. When the source was delivered, it did not have the 500 mCi emission expected. A proper source <u>can</u> be obtained, but would require more time and effort than could be applied under the present program.

4. During the final portion of Phase II the Betasonde was fabricated, tested and calibrated. It meets all of the original design objectives and, with proper radiation source, would be capable of providing density altitude profiles to at least 80 km - 90 km.

As described in Section 1, the final phase of this program would be Flight and Data Analysis. During this phase of the work (not presently funded by the Army Research Office) the instrument must be integrated into an Arcas (or other rocket) payload for launch, and calibrated at both Panametrics and in a large (40' - 60') chamber in order to verify the high altitude ($\gtrsim$ 70 km) portion of the calibration curve. The Betasonde II should then be flown to the 80-90 km region at least twice, and the analytical fitting procedure described above should be applied to the data. This will form the basis for routine direct measurement of atmospheric density up to at least the 80-90 km region, with possible extension to 100 km by use of more intense sources or lower electronic noise electronics. Should this prove to be feasible, as is expected based on the present results, it would then be useful to consider application of the technique up to the 100 km region either by use of a more intense source (several kCi), by developing detection techniques allowing a lower energy threshold ($\lesssim$ 10-20 keV) - combined with a low energy beta source like Ni-63, or a combination of these measures.

Inasmuch as the U.S. Government has a considerable investment in this sonde at this time, we believe that it should be utilized in the flight program recommended above.

REFERENCES

1.1 B. Sellers and J. L. Hunerwadel, Atmospheric Density Measurement in the Middle Atmosphere, PANA-AIR-2 (August, 1977) AD A055 773.

1.2 B. Sellers, F.A. Hanser, and J. L. Hunerwadel, Stratcom VI-A UV Flux and 30 - 65 km Low-Background Betasonde Air Density Measurements, PANA-AIR-1 (July, 1976) ADA055 772.

1.3 B. Sellers, H. N. Ballard and M. Izquierdo, Direct Measurement of Air Density in the 30 - 60 km Region by Beta-Ray Forward Scattering, J. Appl. Rad. Iso. 20, 341 - 351 (1969).

2.1 R. D. Evans, The Atomic Nucleus, McGraw-Hill, NY (1955).

2.2 O. H. Hogan, P. E. Zigman, and J. L. Mackin, Beta Spectra II. Spectra of Individual Negatron Emitters, USNRDL-TR-802 (December 1964) AD455961.

2.3 U.S. Standard Atmosphere 1962. U.S. Government Printing Office, Washington, D. C. 20402 (1962) AD401813.

2.4 U.S. Standard Atmosphere Supplements, 1966, U.S. Government Printing Office, Washington, D. C. 20402 (1966).